Pyroclastic deposits and volcanic edifices record unusually vigorous lava fountains during the emplacement of a flood basalt flow field (The Roza Member, Columbia River Basalt Province, USA)

Richard J. Brown[*], S. Blake, T. Thordarson[1], S. Self

Volcano Dynamics Group, Department of Environment, Earth and Ecosystems, The Open University, Walton Hall, Milton Keynes, MK7 6AA, UK

[1]School of Geosciences, Grant Institute, The King's Buildings, University of Edinburgh, West Mains Road, Edinburgh, EH9 3JW, UK

[*]Now at: Department of Earth Sciences, Durham University, Science Labs, Durham, DH1 3LE, UK

Contact email: richard.brown3@durham.ac.uk

Abstract

The 1300 km^3 tholeiitic lava flow field of the 14.7 Ma Roza Member of the Miocene Columbia River Basalt Group has the best preserved vent system of any known continental flood basalt. Detailed geological mapping and sedimentary logging of the pyroclastic rocks along the >180 km-long vent system has enabled the reconstruction of exposed pyroclastic edifices (partial cones) that built-up around vents. The pyroclastic edifices differ from those constructed during typical basaltic effusive eruptions and may represent a new type of volcanic cone ('agglutinate cones'). They are characterised by low to moderate slope angles (<19°), are composed dominantly of coarse-grained moderately to densely agglutinated and welded spatter and scoria extending up to 750 m away from the vent and had minimum heights of 15–160 m. Thick, well-sorted fall deposits composed of moderately to highly vesicular scoria lapilli extend away from some vents and exhibit some characteristics comparable to the proximal deposits of violent Strombolian or basaltic Plinian eruptions. The recorded volcanic activity does not fit with presently known eruption styles of basaltic magmas and the evidence indicates that the Roza eruption was punctuated by eruptive activity of unusually high intensity that was characterised by vigorous lava fountains. The extensive agglutinated deposits accumulated around the vents as a result of fallout from high (>>1 km) fountains enhanced by fallout from the lower parts of tall convective columns that rose above the fountains.

Keywords: flood basalt, pyroclastic, lava fountain, fissure, volcanic vent

Introduction

Flood basalt eruptions are the most voluminous and longest-lived volcanic events on the planet. Throughout geological time, periodic flare-ups of flood basalt activity have paved large areas of the Earth with lava (10^6 km^2). Due to the huge volume of basalt magma emitted during these eruptions (100s–1000s km^3), and the release of massive amounts of climate-altering gases, these events have been proposed as potential triggers of global climate change and mass extinctions (e.g., Rampino and Stothers, 1988; Thordarson and Self, 1996; Olsen, 1999; Courtillot and Renne, 2003; Saunders and Reichow, 2009; Thordarson et al., 2009). These volatiles released from the magma are intruded into the atmosphere either within ash-bearing eruption plumes or by thermal convection (gas-laden plumes) above pyroclastic fountains (Stothers et al., 1986; Woods, 1993). The height these climate-changing gases reach into the atmosphere along with the duration of eruptions are critical for the longevity and severity of their effect on regional and global climate systems. The deposits of plumes and fountains from fissure eruptions in continental flood basalt provinces have remained elusive due to limited exposure and the huge size of most provinces: proximal pyroclastic deposits may account for <0.001 % of the area covered by a flood basalt flow field and have little chance of being exposed through erosion (see review in Ross et al., 2005).

The best known examples of proximal pyroclastic deposits are from flood basalt fissure eruptions from the Miocene Columbia River Basalt Province (CRBP), USA. Swanson et al. (1975) documented vent deposits and related products for two flood basalt flow fields, the Roza Member and the Ice Harbor Member, and others have since been found (e.g., Reidel and Tolan, 1992). The products comprise shallow-level dikes (10–>600 m paleo-depths) and a range of pyroclastic deposits that form pyroclastic cones and sheet-like fall deposits. Elsewhere proximal deposits have proven useful in deciphering the dynamics of an eruption—something notably lacking for flood basalt volcanism. In this paper, we present the results of detailed field investigations on the best preserved proximal deposits of any known flood basalt eruption: the 15 Ma Roza Member (Martin, 1989; Thordarson and Self, 1996, 1998). We report the results of geological mapping, sedimentary logging and laboratory investigations of the pyroclastic deposits exposed along the >180 km-long Roza vent system. We use this data to reconstruct the volcanic edifices that built-up around the vents during the eruption, and we then discuss what they tell us about near-vent processes during flood basalt eruptions. We show how the Roza vent system as a whole is comparable to those constructed during historic basaltic fissure eruptions on Iceland. But we demonstrate that the edifices are markedly different to those constructed during Hawaiian-Strombolian style monogenetic eruptions (i.e., spatter or scoria cones) in both morphology and lithology. Indeed, they may constitute a new type of volcanic landform (here termed ‘agglutinate cones’) characterised by moderate slopes (<20°) and by being composed of predominantly welded and agglutinated scoria and spatter layers that extend >500 m away from the vent in some cases. We propose that they formed during eruptions that were typified by periodic vigorous lava fountaining and associated strongly convecting plumes that may have exceeded Subplinian intensities at some fissure vents. The geological evidence presented suggests that flood basalt eruptions were periodically capable of transporting climate-changing gas species high into the atmosphere (Stothers et al., 1986; Thordarson and Self, 1996).

Geological Setting

The intermontane Miocene CRBP consists of > 230 000 km^3 of basalt lava (Camp et al., 2003). Surface effusion of what are classed as CRB lavas was initiated c. 17 Ma ago in the Steens Mountain area in Oregon following impingement of the Yellowstone hotspot on the western edge of North American lithosphere (Camp and Ross, 2004). Lavas were possibly fed by 300 km-long dike swarms that originated in 15–30 km deep crustal chambers in east-central Oregon/west-central Idaho (Wolff et al., 2008; Fig. 1A). The last CRBP eruptions occurred in the central part of the CRBP at 6 Ma (the Pasco Basin; Tolan et al., 1989; Tolan et al., 2009).

The crust under the CRBP in SE Washington is composed of complex accreted Late Paleozoic and Mesozoic intraoceanic terranes and Proterozoic continental crust. Accretion is thought to have occurred from 135–90 Ma (e.g., Lund and Snee, 1988). The boundary between accreted terranes and continental crust is a complex suture zone—the Western Idaho Suture Zone (WISZ). Oblique subduction of the Juan de Fuca plate generated horizontal NNW–SSE compression and E–W extension during the Miocene, which resulted in NNW–SSE propagation directions for CRBP magma in dikes through Oregon and SE Washington (Reidel, 1984; Hooper and Conrey, 1989).

Methods

Pyroclastic deposits were mapped at a 1:5000 scale and geospatial data were recorded on a hand-held GPS. Detailed measured sections were made of well-exposed outcrops. Conventional methods of grainsize analysis are not applicable due to agglutination, and the variable degree (low to moderate) of alteration and lithification seen in most outcrops. One-hundred-and-fifty samples were taken for rock density measurements, which were carried out in the laboratory following the method outlined by Houghton and Wilson (1989). At many locations the bedding dips and strikes define partial pyroclastic edifices. Horizontal dimensions for these edifices are estimated and given as radius (orthogonal to inferred alignment of the vent system) and length (parallel to inferred axis of vent system).

The best exposures are man-made sections, either road or rail cuts or quarries. Most natural outcrops occur along the floors of glacial flood channels (the ‘channelled scabland’), and lack exposure of the tops and bottoms of units. Mapping individual fall horizons over more than a few 10s meters to 100 m is difficult because of intermittent exposure and rapid lateral and vertical gradations, on a decimeter to a meter scale, from loose scoria through to lava-like densely welded spatter that lacks outlines of constituent clasts.

The Roza Member vent system

The 14.7 Ma Roza Member is a 1300 km^3 flood tholeiitic basalt flow field covering ~ 40 300 km^2 of SE Washington and NE Oregon (Martin, 1989; Tolan et al., 1989; Thordarson and Self, 1998). It was erupted from a linear vent system (Fig. 1) that presently outcrops discontinuously for >180 km from just north of Enterprise in NE Oregon to north of Rock Creek in SE Washington (see also Swanson et al., 1975). It can be divided into two segments: south and north of the Snake River. South of the Snake River, the vent system is represented by dikes trending N17°W, pyroclastic deposits and clastogenic lavas. Pyroclastic deposits and proximal lavas are generally poorly exposed south of the Snake River (Fig. 1A) and consist of thick accumulations of spatter, pyroclastic breccia, spongy pāhoehoe lobes, and thin to thick, dense lava. In some cases these form small (from ~ 1 to 2 km wide) shield-like edifices (e.g., Little Butte and Big Butte, Swanson et al., 1975).

North of the Snake River, the location of the Roza Member vent system is recorded by proximal pyroclastic deposits and spongy pāhoehoe lavas that accumulated around vents along fissures (Swanson et al., 1975). They are better exposed than outcrops south of the Snake River because of the scouring by the great Pleistocene-age Missoula Lake floods (Bretz et al., 1956). In this study eight new vent areas have been recognised at the NW end of the vent system (Fig. 1B), bringing the total number of exposed fissure-vent segments recorded north of the Snake River to eleven (including those of Swanson et al., 1975). These pyroclastic accumulations have an apparent spacing of 1–5 km, although this is somewhat controlled by the degree of exposure, and more are potentially buried under younger lavas and other deposits (e.g., Pleistocene-Recent glacial loess). The discovery of new vent deposits to the north of those identified by Swanson et al. (1975) now clearly indicates that the Roza fissure north of the Snake River strikes N40°W. The pyroclastic deposits outcrop within a 3 km-wide along-strike zone. Projecting this N40°W trend south-eastwards, it intersects dikes that trend N20°W–N30°W along the banks of the Snake River, indicating a 23° counter-clockwise deflection of the dike-vent system over an along-strike distance of < 5–10 km (Fig. 1B).

Proximal pyroclastic deposits

A complete spectrum of pyroclastic lithofacies is exposed along the Roza vent system, from loose scoria fall deposits through to densely welded spatter and clastogenic lava. Lithofacies have been drawn out of this spectrum of deposits on the basis of composition, texture, rock density, grainsize, and clast aspect ratio. Lithofacies descriptions and interpretations are summarised in Table 1 and representative photographs are given in Figure 2. When exposed, pyroclastic deposits are in general well preserved and are only weakly to moderately altered (mostly clay replacing glass). Primary textures (e.g., vesicles) and features (e.g., achneliths) are well preserved in some outcrops (Fig. 3B). The locations of individual Roza vents have been constrained primarily by: (A) a lithofacies association that comprises scoria, moderately to densely agglutinated scoria and spatter, lava-like densely welded spatter and clastogenic lava; (B) dipping strata that defines pyroclastic edifices; and (C) the presence of abundant spatter bombs up to 1 m in diameter indicating deposition under a fountain. In this paper we follow the terminology outlined by Wolff and Sumner (2000). We use the term ‘agglutinated’ to describe clasts that have stuck together on deposition. We use the term ‘welded’ to describe scoria and spatter deposits in which clasts have agglutinated and have subsequently partially to totally lost their outlines and undergone a strong degree of compaction flattening. The term ‘clastogenic lava’ is reserved for a flow composed of partially coalesced pyroclasts. We have divided the Roza pyroclastic deposits into different classes dependent on average bulk rock densities, clast aspect ratios and grainsize (Table 1).

At most localities where the base of the Roza pyroclastic deposits is visible, they overlie pāhoehoe lavas of the Roza Member. Below we describe the most instructive and best-exposed outcrops of pyroclastic deposits associated with each vent segment, from north to south, in terms of their stratigraphy, geometry and lithofacies associations. We also describe the Roza lavas that buried, and led partially to the preservation of, the pyroclastic deposits. Useful details from poorer quality outcrops are summarised in Table 2.

Buffalo Spring North (BSN)

The Buffalo Spring North vent construct lies 900 m south-southeast of the northernmost exposed Roza vent accumulations (the poorly exposed Harder Ranch vent; Fig. 1B, Table 2). It is an eroded pyroclastic edifice comprised of weakly to densely agglutinated scoria and spatter and lava-like densely welded spatter (Table 1 and Fig. 4B) exposed over 0.3 km^2. Bedding and agglutination fabrics dip 6–35° to the SW, W and NW and define the western side of an edifice with an apparent radius of >330 m and a minimum length of 560 m (Fig. 4B, Table 3). The bulk of the exposed pyroclastic deposits are densely agglutinated scoria and spatter (lithofacies dwScL, dwSpB) and lava-like densely welded spatter (lithofacies llwSp; Fig. 2D-F) in beds several decimeters to several meters thick. Spatter bombs within the deposits reach 1 m in diameter. Rheomorphic flow of some lava-like spatter beds is indicated by brecciated vesicular layers and centimeter-scale tension gashes.

Buffalo Spring South (BSS)

Pyroclastic deposits of the Buffalo Spring South vent construct outcrop 700 m south-southeast of the BSN and cover 0.06 km^2 (Fig. 4A and C). Dips of beds (or bedding planes) vary from 8–31°, with an average ~ 16° and define the NE, E and SE portions of a small volcanic edifice. The edifice is elongated in a NW–SE direction and the preserved (exposed?) part has a radius of 130 m and a length of 280 m (Table 3). Inward-dipping strata define the position of the crater, while the SW portion of the cone passes into an area of non-systematic dips and strikes (Fig. 4C). The NW portion of the construct is not preserved. The edifice is comprised of bedded moderately and densely agglutinated scoria lapilli and spatter. The stratigraphically oldest deposits exposed are black, lava-like densely welded spatter. Vesicular spatter bombs are conspicuous and reach 1 m long and are common within beds of oxidised moderately agglutinated scoria (e.g., Fig. 3C). The bombs have aspect ratios of 1:2–1:10 and are non- to moderately vesicular (<55 vol. %) and typically have black interiors and brown, altered glassy exteriors with ropy and fluidal textures.

Rock Creek Center (RCC)

A > 50 m-thick sequence of pyroclastic deposits is exposed along the eastern bank of Rock Creek (Fig. 5). The succession drapes a series of earlier Roza sheet lobes that vary in thickness from 10 m in the north to 25 m in the south, over a distance of 400 m (Fig. 5A). The pyroclastic succession consequently thins to the south over the lavas and appears to merge with the pyroclastic deposits of the RCE vent (Fig. 5A). The sheet lobes are the oldest Roza products exposed in Rock Creek and they locally pass upwards into 3 m of lava-like densely welded spatter and thin clastogenic lava flows (Fig. 6). This is overlain by a 1.5 m thick lithic breccia comprised of angular blocks and boulders, and of densely welded Roza spatter, similar to the underlying deposits (Fig. 6). The lithic blocks and boulders are composed of Roza lava. This is overlain by a well-sorted 2 m-thick scoria fall deposit that gradually fines upwards. The upper meter of the fall deposit is densely welded without any observable increase in grainsize. This would suggest an increase in accumulation rate during deposition of this welded part of the bed. This is sharply overlain by 6 m of clastogenic lava and vitrophyric spatter (Fig. 6). The upper ~ 35 m of the succession is dominated by red oxidised weakly and moderately agglutinated scoria (ScL and waScL, Table 2) in massive or diffusely bedded units that range in thickness from < 1–15 m thick. Thinner intercalated agglutinated beds (waScL; Table 1) typically show poorly developed columnar joints. Beds in this succession dip 10–22° to the north, east and west and define a half cone with an estimated minimum radius of 250 m and a minimum length of 430 m (Fig. 5C and Table 3). The vent that emitted these pyroclastic deposits is inferred to sit under Rock Creek and is probably aligned NNW–SSE (Fig. 5).

Rock Creek East (RCE)

Pyroclastic deposits of the Rock Creek East vent outcrop over 1.15 km^2 of channelled scabland to the east of the track that leads into Rock Creek (Fig. 1 and 5D). At the southeastern end bedding dips and strikes outline a pyroclastic edifice estimated to be ~400 × 500 m in diameter (Fig. 5D, Table 3). The center of the edifice is cut by a 70 m-wide channel filled with alluvial sediments: we infer that this is coincident with the position of the vent around which the edifice was constructed. Beds dip 13–44° east and north. Less well-exposed pyroclastic deposits dip 10–21° to the south on the southern flank of the edifice (Fig. 5B). Lower parts of the northern and southern flanks of the edifice are comprised of black lava-like and densely welded spatter. This passes up into lower grade densely-welded and moderately agglutinated scoria and densely welded spatter that makes up the bulk of the preserved northern flanks (Fig. 5B). There are several small outcrops of densely welded spatter in the channel that dip inwards at steep angles (44–65°): these are inferred to be deposits that have slumped into the vent (not exposed) or that mantled the steep interior crater walls of the edifice. Later-emplaced Roza sheet lobes onlap against the cone and completely cover it to the south; discordant relationships between steeply dipping strata and horizontal sheet lobes on the east side of the vent indicate that the crater was also inundated by lava.

Bedded pyroclastic deposits extend 500 m to the north of the edifice and outcrop over an area of 0.15 km^2. Dips and strikes of bedding and welding fabrics are non-systematic and change rapidly (Fig. 5D). Dips vary from 0–60° in all directions but do not outline obvious cones or partial cones. Individual beds cannot be traced laterally due to rapid changes in dip and strike, limited exposure, and rapid changes in agglutination intensity. Vents have not been recognised in this area and we infer that the pyroclastic deposits were erupted from the same vent that constructed the cone to the south, thus were dispersed up to 700 m from this vent area.

It is of interest to note that the vent that fed RCE appears to lies ~1 km east (orthogonal to fissure axis) of the vent that fed RCC (Fig. 5A), suggesting an en echelon arrangement of fissures.

Texas Draw (TD)

The Texas Draw vent area (Fig. 1 and 7) is marked by bedded weakly to densely agglutinated scoria and spatter exposed over an along-fissure distance of 1 km and an area of >1.6 km^2. The base of the pyroclastic succession is not seen. In northern areas, bedding and welding fabric orientations define an edifice with slopes generally dipping 16–34° to the north, west and south (Fig. 7A, B and E). We infer that this edifice was constructed on the western side of a ~N–S-trending vent that ran down the valley. An eastern counterpart to this edifice is missing and post-pyroclastic phase lavas are instead exposed (Fig. 7B). In detail the dips and strikes within this edifice are complicated. Dip direction and magnitude change rapidly over distances of 10's of meters and define significant smaller-scale topography (Fig. 7B). A 60 m-wide depression demarcated by inward-dipping beds is present on the inner side of the edifice at the north and may represent a slump scar mantled by pyroclastic fall deposits (Fig. 7A). Up to 30 m thickness of continuous pyroclastic deposits are exposed at the southern end of the edifice (Fig. 7C). The lower 15 m comprises bedded brown to red weakly to densely agglutinated bedded scoria with large spatter bombs (< 40 cm in diameter, Fig. 7C). Moderately agglutinated scoria beds tend to form discontinuous lenses 5–50 cm thick and up to 5 m wide. This passes upwards into a succession dominated by densely agglutinated scoria and spatter. Several thick beds of densely agglutinated scoria are persistent over hundreds of meters and exhibit columnar joints spaced ~ 10–50 cm apart. The upper ~ 15 m consists of higher grade pyroclastic deposits (densely agglutinated scoria and spatter and lava-like densely welded spatter), in beds from < 1m to > 5 m thick. Changes in welding grade are abrupt (Figs 6 and 7) and individual pyroclastic fall layers pinch out or change character (e.g., in degree of agglutination) markedly over lateral distances of several 10's–100's of meters (Fig. 7).

To the south and southeast of the edifice, dips and strikes are much less systematic and individual edifices are more difficult to define. The exposed thickness of the pyroclastic deposits exceeds 10 m in places and dips vary from 0–45° and change magnitude and direction rapidly. Several ridges with broadly opposing dips are present (Fig. 7B) but there is no direct evidence for vents or craters. The complicated nature of the Texas Draw outcrops suggests that the pyroclastic deposits may be the products of more than one sub-parallel or en echelon vents.

The pyroclastic beds are partially overlain by columnar jointed Roza sheet lobes (Fig. 7A and B), of which typically only the cores are exposed (upper crusts have been eroded and bases are not seen).

Mason Draw (MD)

Pyroclastic deposits at Mason Draw (Fig. 1) are exposed over an area of at least 5 km^2. Most outcrops are small (several meters wide), of poorer quality than those described above and comprise moderately to densely agglutinated scoria and spatter outcropping over 2.6 km^2. The base of the pyroclastic deposits and of the Roza Member is not exposed. Bedding dips and fabrics dip 10–27° to the S, SW and NW and define an edifice similar to that at Texas Draw. This edifice is elongated approximately north-south. Consistent westward dips suggest that the edifice had a radius of 500 m and a length of >500 m. We infer that it built up around a vent located beneath the present valley floor. The western rim lacks an eastern counterpart and Roza sheet lobes outcrop at the same stratigraphic level on the other side of the valley. The cone (or spatter rampart) passes westward and northward into variably agglutinated pyroclastic deposits that, as at other vents, exhibit non-systematic and rapidly changing dips and strikes. Locally, steeply-dipping densely welded spatter beds record slumping of hot pyroclastic deposits. The edifice is overlain by Roza sheet lobes to the north, although horizontal-bedded pyroclastic deposits are exposed 500 m north of the edifice (Fig. 1). Wedges of weakly to moderately welded scoria and densely welded spatter occur on top of Roza sheet lobes NE of the Mason Draw vent deposits.

Winona (WI)

Pyroclastic deposits representing the Winona vent accumulations (Fig. 1) are primarily exposed in discontinuous, but in total 3 km-long, east-west trending road and railroad cuts. This set of exposures provides a section through a vent and examples of pyroclastic fall deposits inter-bedded with thin pāhoehoe lavas. Both the fall deposits and the lavas are inferred to have been sourced at the vent. The lowermost exposed products of the Roza Member in the Winona area are pāhoehoe lobes with thick rubbly, highly vesicular upper crusts and dense, columnar jointed cores. They are best exposed in man-made sections in roads as small lobes several meters to several 10's m wide and up to 8 meters thick (Fig. 8A and B). The upper crust on these lobes is up to 5 meters thick, indicating emplacement times of ~6 months (Hon et al., 1994). The upper surfaces of these lavas in one area exhibit tumuli spaced >10 meters apart with relief of several meters. Source vents for these early Roza lobes in this area are not known.

Rail cuts west of Winona, that parallel the south bank of the Palouse River provide a cross-section through the vent system, which here consists of two opposing mounds of outward-dipping densely agglutinated spatter (Fig. 8B). The western mound comprises > 10 m of densely welded spatter (Fig. 8C) that dips 5° towards the east and is exposed for 140 m along the railway track. It has a wedge-like morphology in cross-section and tapers to the east. The base and top of this spatter unit are not exposed but the grade of welding decreases upwards and also decreases eastwards, although exposure is broken. The mound has a steep eastern margin that abuts against two columnar jointed Roza sheet lobes (Fig. 8B). The sheet lobes sit within a 160 m wide depression that is bound on its western margin by a westward tapering mound,~400 m wide, of densely welded and lava-like spatter similar to that already described. Welding fabric within this second wedge dips 7° to the west. We infer that these two wedges constitute a low-profile spatter cone constructed either side of a vent that subsequently filled with Roza lava. Vertical welding fabrics are present within some parts of these wedges and may have formed during slumping or mantling of crater walls. Mounds of weakly to moderately agglutinated scoria and densely welded spatter outcrop on top of a Roza sheet lobe over a wide area at the western end of the railway section at Winona (rafted spatter on Fig. 8A). Adjacent mounds show diverging bedding and welding fabric dips, however the continuation of the deposits in 3D is not known.

Well-sorted scoria fall deposits outcrop at several places around Winona. At the eastern end of the railway section, and in road cuts 1.7 km to the east of the vent, at the same stratigraphic horizon as the densely welded spatter mounds, is an ~8 m thick sequence of scoria fall deposits and vesicular rubbly lavas (see Thordarson and Self, 1996, 1998). Overlying the lowermost Roza lavas are two clast-supported, well sorted scoria fall deposits separated by a vesicular rubbly pāhoehoe lobe. The fall deposits are each > 2 m thick and are un- to moderately altered. The fall deposits are massive apart from several thin (5–6 cm thick) finer-grained horizons. Where unaltered they comprise well-sorted black scoria lapilli up to 5 cm in diameter. The scoria lapilli have densities of 300–1100 kg m^{-3}, equivalent to vesicularity values of 65–90 vol. % (Fig. 9C). Modal values are 500–600 kg m^{-3} (80–84 %). Clasts exhibit numerous small spheroidal vesicles (Fig. 3A) and have fused exteriors and fractured surfaces (Thordarson and Self, 1998). The Roza fall deposit is in its physical properties very similar to the tephra from the explosive phases of sub-Plinain intensities produced by the 1783-84AD and 934-40 AD Eldgjá flood lava eruptions (e.g. Thordarson and Self, 1993; Thordarson et al., 2001). Clast morphologies (including achenliths) and vesicularities (between 75-90 vol% in all cases) are comparable and so is the grainsize distribution of the proximal tephra (Fig. 9D). We infer that these fall deposits coarsen eastward into the densely agglutinated spatter mounds at the Winona vent, 1.7 km to the west. The scoria fall deposits under and above the rubbly lava have been disrupted into a series of meter-scale mounds ('pumice ramparts' of Swanson et al., 1975) by continued movement of the lava beneath during and immediately post deposition.

Correlating fall deposits across the region is difficult due to the monotonous nature of their physical characteristics, the weak, locally absent bedding, the rapid lateral facies changes close to inferred vents, and the intercalated pāhoehoe lavas that diachronously dissect the deposit and are themselves not possible to correlate between outcrops. The upper contact of the fall deposit is invariably welded to a depth of 5–15 cm, and commonly thermally discolored (oxidised) to a depth of a meter or more, and exhibits ~ 10 cm-spaced curving columnar joints as well as thermal discoloration. The density of the fall deposits increases up through the welded zone from 950 kg m^{-3} to 1550 kg m^{-3} over 35 cm. In the thicker sections of the fall deposits it is not uncommon to find intercalated thin spongy pāhoehoe lobes; these are typically less than a meter thick. At some locations the fall deposit grades down into > 5 m of coarse-grained non- to moderately-agglutinated scoria with coarse bombs.

Post-pyroclastic-deposit lava flows

The pyroclastic edifices along the Roza vent system are onlapped by 1–5 horizontal Roza sheet lobes (e.g., Figs. 4 and 5). These lobes are typically between 1–20 m thick, with classic tripartite lower crust, core and upper crust divisions of pāhoehoe lavas (Thordarson and Self, 1998). The upper crusts of these sheet lobes are widely in excess of 6 m thick and are defined by decimeter to meter thick diffuse vesicle bands. Emplacement times for these lobes are in the order of 9–12 months (based on empirical model of upper crust growth of Hon et al., 1994; see also Thordarson and Self, 1998). It seems probable that only the largest edifices of pyroclastic deposits remained unburied by Roza sheet lobes. At the base of some sheet lobes are packages of centimeter- to decimeter-thick vaguely defined vesicular pāhoehoe lobes with thin glassy and partially annealed crusts. These packages can reach several meters thick. Gas blisters up to 70 cm high occur beneath crusts in some sheet lobes. The southern end of the Mason Draw edifice is overlain by several meters of thin, spongy and shelly pāhoehoe lobes. Shelly pāhoehoe consists of lobes that are < 50 cm thick, < 1 m wide and have large gas cavities beneath the thin crusts. Rafted mounds of moderately and densely agglutinated spatter occur on top of sheet lobes to the NW of the edifice.

At several off axis locations along the fissure (e.g., western end of Winona railcut, Fig. 8A and B) small mounds of rafted variably oriented weak to moderately welded and agglutinated scoria overlie the upper sheet lobes. The upper surface of the lava must have exhibited considerable relief (2–4 m) as meters-thick beds of scoria and spatter occur at the same level as exposed sheet lobe cores. Bedding defined by fabrics in these pyroclastic deposits dips non-systematically. At one locality, it appears that the bedded spatter and scoria drape 5 meters of relief on the margin of a sheet lobe.

Interpretation

Spacing of pyroclastic cones along the Roza fissure

At least 11 separate vents have been identified from surface pyroclastic deposits over a distance of ~ 32 km (Fig. 1). The spacing of large Roza pyroclastic cones is 0.8–4 km, with an average of 2 km. The average spacing of large cones along the Roza fissure is similar to that along the 27 km-long Laki fissure, Iceland, where large pyroclastic constructs are spaced 0.5–5 km apart (average 1.5 km; Thordarson and Self, 1993). Incomplete exposure and the burial of pyroclastic deposits by later-erupted Roza lavas, plus parts of the fissure covered by younger sediments, including loess, inhibit a full understanding of the number and spacing of vents along the fissure. At Laki, pyroclastic cones and spatter ramparts occur nearly continuously along the entire length of the fissure; 70 separate vents were active along the 4.5 km-long fissure during the 1983 eruption of Miyakejima (Aramaki et al., 1986). However, the similarity in terms of vent spacing and cone dimensions between the Roza and the Laki eruptions suggests overlap in physical processes and that Laki makes a reasonable first-order analogue in this respect for the Roza vent system. The Roza agglutinate cones may have lithological similarities to the proximal deposits of the 934 AD Eldgjá eruption on Iceland (Thordarson et al., 2001).

The position of the vents along the Roza fissure is precisely known, but large discrete outcrops of densely agglutinated spatter and coarse spatter bombs occur over zones up to 1–4 km wide orthogonal to the trend of the fissure (e.g., Winona and Rock Creek, Fig 1B). This suggests that activity may have occurred locally from several sub-parallel overlapping fissure segments (e.g., Fig. 5) spread across a zone up to several kilometres wide. This is unusual compared with historic fissure eruptions which have come from very narrow zones, << 1 km (e.g., Miyakejima volcano, Japan, Aramaki et al., 1986; Laki, Iceland, Thordarson and Self, 1993).

Reconstruction of proximal pyroclastic constructs

A range of edifice constructs are present along the Roza fissure, from broad, probably lava-dominated (but very poorly exposed) cones/shields (e.g., Big Butte and Little Butte, Table 2), through to pyroclastic edifices composed dominantly of agglutinated spatter and scoria (e.g., BSN, BSS, RCC, RCE, TD, MD and WI). It is the latter upon which we focus this discussion. The pyroclastic edifices are composed of a range of pyroclastic deposits. The characteristics of the Roza pyroclasts, including the coarse grainsize, abundant fluidal-shaped clasts, scoriaceous clasts, spatter bombs, achneliths (Pele's tears) (Table 1 and Fig. 2) are typical products of strong gas-driven fire fountain activity in basaltic eruptions of all scales. Proximal pyroclastic sedimentation is inherently unsteady (e.g., Head and Wilson, 1987; Houghton et al., 2004) and fluctuations in gas content, pyroclast grainsize, accumulation rate, and fountain height, structure, orientation and temperature can result in complex lateral and vertical sequences of pyroclastic deposits. Such unsteadiness accounts for the abrupt vertical and lateral changes in agglutination state and grainsize within the Roza proximal deposits (see Figs. 6 and 7). Beds of densely agglutinated scoria commonly show columnar joints (e.g., Fig. 2) indicating that they were emplaced rapidly and then cooled as single units. Closely-spaced platy jointed units at the base of some lava-like densely welded spatter are similar to those at Puʻu ʻŌʻō, Kilaeau, interpreted by Heliker et al. (2003) as shear planes beneath clastogenic lava flows.

The radii of preserved Roza pyroclastic edifices, orthogonal to the inferred axis of the fissure vent system, are > 200–400 m and their lengths parallel to the fissure are > 280–900 m. Around most Roza vents bedding dips of pyroclastic deposits and dips of welding fabrics are in the range 4–34°, with mean values of 15–19° (Fig. 9A). The deposits crudely define partial cones with outward radial dips over sectors of <180°. Geometric reconstructions using these dimensions and the dips of bedding planes and welding fabrics give restored edifice heights of 15–160 m (Table 3) and volumes of pyroclastic cones in the range of 10^{-4} to 10^{-2} km^3. If we assume that cones, both small (50%) and large (50%), are spaced 1 km apart along the 300 km-long Roza fissure, then a minimum volume of pyroclastic material preserved as cones is ~ 10 km^3 (< 3–5 km^3 DRE). We infer that an equivalent volume was dispersed widely as ash and scoria fall deposits during the eruption. This is equivalent to < 1% of the total erupted volume of the Roza Member. We refer to these cones as ‘agglutinate cones’ to distinguish them from scoria cones and spatter cones.

Many of these agglutinate cones appear to be elongated in N–S or NNW–SSE directions (Table 3), which is consistent with the overall trend of the Roza vent system. Several appear to have built up preferentially on one side of the inferred vents with opposite parts missing (e.g., TD, MD vents). Their absence could be due to deposition from strongly wind-sheared plumes, from deposition from angled fountains, or from the rafting away of large sectors of the cone on top of lava flows. Evidence for rafting is seen at Mason Draw, Winona and Palouse River vents (Fig. 1). Around several of the vents the pyroclastic edifices pass laterally into extensive areas where bedding orientations are non-systematic and change rapidly in dip and strike (e.g., RCE, TD and MD vents). These regions cannot easily be explained as areas where neighbouring cones converged and overlapped (as is common along fissures, Thordarson and Self, 1993; Sable et al., 2006) because dips are extremely variable. Instead, such areas are consistent with the draping of irregular topography (formed by subjacent sheet lobes and hummocky pāhoehoe flows) by sheet-form welded and agglutinated fall deposits. At Rock Creek Center these deposits extend up to 750 m away from the vent (Fig. 5); at Mason Draw they extend > 500 m from the vent.

Few of the agglutinate cones preserve crater deposits. Steep, inward-dipping strata at Rock Creek East and Buffalo Spring South are inferred to be agglutinated spatter that is either mantling crater walls or has slumped into the crater or vent (Figs 4 and 5). Several poorly exposed crater deposits outcrop south of the Snake River (e.g., Potter White Hill and Crow Creek, Table 2). These comprise lithic clast-rich agglutinate breccias and densely agglutinated spatter. They show evidence for slumping and commonly have steep contacts between adjacent pyroclastic units.

The dimensions of the Roza agglutinate cones are comparable to scoria cones formed during both small monogenetic basaltic eruptions (e.g., Porter, 1972; Wood, 1980) and larger basaltic fissure eruptions (e.g., cones along the 1783–5 Laki fissure eruption, Iceland, Thordarson and Self, 1993). However, the Roza edifices differ from scoria cones in two important ways. First, they are composed dominantly of welded and agglutinated spatter and scoria, even at distances of > 400 m from the vent. Loose, non-welded/agglutinated scoria deposits account for only a small volume of the preserved cones—the edifice at the Rock Creek Center vent has the thickest succession of low-grade pyroclastic material with >30 m of weakly to non-welded scoria (ScL, waScL; Fig. 6). Typically non-welded/agglutinated pyroclastic deposits are absent or account for only a small volume of each edifice. It is not the case that overlying loose accumulations of typical scoria cone deposits have been eroded because later Roza onlap onto these edifices at several locations (e.g., RCE, RCC, TD, MD and WI). Thus, in many instances the preserved deposits more or less represent the entire pyroclastic construct. Second, the mean dips of beds and welding fabrics in the Roza edifices (Fig. 9A) are considerably lower than those typical of scoria cones, which are commonly at the critical angle of repose for loose scoria as a result of grainflow (~ 35°, Wood, 1980). These two characteristics set apart the Roza edifices from most pyroclastic cones constructed during basaltic eruptions, and are indicative of phases of vigorous fountaining. Fountains during Hawai‘ian eruptions typically range from 100–500 m in height, spatter-rich accumulations are commonly limited to ultra-proximal regions and spatter cones typically extend only meters to tens-of-meters from vents and may reach a few 10s of meters high (e.g., Thordarson and Self, 1993; Parcheta et al., 2012).

Individual fall layers are not traceable away from the Roza vents and thus isopach maps cannot be constructed with which to extract quantitative measures of pyroclast dispersal (e.g., thickness half-distance, b_t, Pyle, 1989). In the absence of this information a useful measure is the linear thickness half-distance — the distance over which a fall deposit halves in thickness away from source ($t_{1/2}$, Houghton et al., 2004). For example, linear thickness half-distance values for Hawaiian-Strombolian cones are 6–30 m (Sable et al., 2006). These values can be calculated crudely for packages of Roza fall deposits that constitute the remnant cones by using the geometric and structural data in Table 3. Roza fall deposits have $t_{1/2}$ values of ~110–200 m. This, of course, bundles together fall deposits that may have widely varying $t_{1/2}$ values, that show varying degrees of welding or agglutination, and that may include clastogenic lava flows, so they must be interpreted with care. Such $t_{1/2}$ values are comparable to those from the more widely dispersed proximal fall deposits from the 1886 basaltic Plinian eruption of Tarawera, New Zealand (Sable et al., 2006).

Discussion

Fountain and eruption dynamics

The unusual characteristics of the Roza edifices, defined by widespread agglutinated and welded deposits, low to moderate slope angles, and $t_{1/2}$ distances of 110–200 m, suggest deposition from tall, vigorous fountains and sustained convection columns (Fig. 10). The evidence suggests that the intensity of eruptions at Roza vents was periodically much higher than is typical for effusive basaltic eruptions. For example, the maximum heights of fire fountains on Hawaiʻi are commonly <500 m, occasionally reaching 800 m (e.g., Wolfe et al., 1988; Sparks et al., 1997): a 400 m-high fountain typically has a basal diameter of <150 m. Fountains of this height only sustain weak convective ash-laden plumes, and the cones that form around them are composed predominantly of loose scoria clasts (e.g., the Puʻu ʻŌʻō cone, Hawaiʻi, Heliker et al., 2003). Deposits from higher intensity basaltic eruptions include those of the 1886 eruption of Tarawera, New Zealand (Walker et al., 1984; Sable et al., 2006). The $t_{1/2}$ values of some of the Tarawera deposits compare well with those of the Roza: Sable et al. (2009) interpreted them as a result of sedimentation from low portions (1–4 km height) of buoyant Plinian columns (lower convective regions and momentum driven jet regions) as the pyroclast release heights were greater than those typically reached by lava fountains or Strombolian eruptions. Abnormally high lava fountains (1.6 km) during the 1986 basaltic andesite-basaltic eruption of Izu-Oshima volcano, Japan, fed a Subplinian plume that reached 16 km high (Sumner, 1998; Mannen and Ito, 2007). During the 1783–5 eruption of Laki, Iceland, fountains reached 0.8–1.4 km in height and produced Subplinian columns of up to 15 km height. High fountains have been invoked to account for the occurrence of rheomorphic lava and densely to poorly welded spatter deposits up to 1.5 km from the vents of the Biskupsfell fissure eruption at Kverkfjöll, Iceland (Karhunen, 1988).

High pyroclast accumulation rates (> 20 cm/min) are needed to cause pyroclasts to weld and agglutinate on deposition (Sparks and Wright, 1979; Thomas and Sparks, 1992). Sable et al. (2006)

calculated average accumulation rates of 15–20 cm/minute for the mostly non-welded Tarawera deposits (see also Walker et al., 1984). These are comparable to the 17 cm/min average accumulation rates of the cone-building phase of the 1986 eruption of Izu-Oshima volcano, Japan (Sumner, 1998). For the Roza eruptions these rates must have been achieved and exceeded at distances of up to 500 m from the vent for extended periods. In order to achieve this the Roza fountains needed to be high (>> 1 km) and sedimentation from the fountains needed to be enhanced by fallout of coarse, hot pyroclasts from the lower parts of associated convecting plumes of potentially Subplinian to Plinian intensity (e.g., Thomas and Sparks, 1992; Sable et al., 2009). Average accumulation rates of ~ 20 cm/min would give construction durations of up to 5–13 hours for Roza cones, which are comparable to the estimated durations of basaltic Plinian and Subplinian eruptions elsewhere (e.g., Sable et al., 2006; see Houghton and Gonnermann, 2008).

The thick sheet-form scoria fall deposits preserved at distances of > 0.1–1.7 km from the Roza vents are interpreted as the products of the sustained plumes developed above the fountains. Poor lateral exposure makes it difficult to correlate individual scoria fall deposits and isopach maps cannot be constructed; intercalated pāhoehoe lobes at many localities further complicate the stratigraphy. The massive to weakly bedded nature of the deposits indicates deposition from semi-sustained, quasi-steady, pulsating plumes (rather than intermittent Strombolian eruptions). At Winona individual fall layers reach > 2 m thick at > 1.5 km from source. These deposits and the characteristics of the pyroclasts are comparable to documented basaltic Subplinian and Plinian fall deposits elsewhere (e.g., Walker et al., 1984; Thordarson and Self, 1993; Costantini et al., 2009, 2011), however there are insufficient outcrops to construct isopach maps and constrain their dispersal.

Whilst welded and agglutinated fall deposits occur in the proximal deposits of all of the modern examples highlighted above, they are not as dominant or as widespread as in the Roza example (cf. Sable et al., 2006), and we have yet to find documentation of comparable volcanic edifices in the literature. We interpret this to mean that eruptions at the Roza vents were periodically characterised by eruptions with unusually vigorous, tall fountains that were most probably topped by sustained and tall convective columns (Fig. 10). These may have been comparable to other documented examples (e.g., Tarawera, Laki and Izu-Oshima eruptions). Explosive basaltic eruptions of Subplinian scale or larger have received a lot of interest recently, (Houghton et al., 2004; Sable et al. 2006; Vergniolle and Caplan-Auerbach, 2006; Constantini et al., 2009, 2011) but there is much that remains unknown (see review in Houghton and Gonnermann, 2008). The geometry and lithology of the Roza edifices are compatible with growth during eruptive phases of substantially higher intensity than is normally associated with lava-dominated basaltic eruptions (i.e, that of typical Hawaiian-Strombolian activity). Controls on the explosivity of basaltic eruptions have been linked to bubble rise and coalescence, degassing processes and melt rheology driven by microlite crystallisation (Houghton and Gonnermann, 2008). An in-depth discussion of the parameters controlling more vigorously explosive phases of the Roza eruption is beyond the scope of this paper and will be dealt with in a future publication.

Eruption scenario at a Roza vent

The Roza fissure is considered to have unzipped from the south to the north based on the geochemical stratigraphy of the stacked sheet lobes in the lava flow field (Martin, 1989). Lavas flowed north and west (until the last phase of the eruption) inundating the paleo-surface in advance of the propagating fissure segments. The base of the Roza Member is rarely exposed north of the Snake River and is not seen at any of the outcrops exposing pyroclastic material; the inference is that activity at several vents appears to have taken place through earlier-emplaced Roza lavas. At Winona, Rock Creek and Union Flat Creek (Fig. 1) the pyroclastic deposits overlie Roza lava indicating that the area was already partially inundated by hummocky pāhoehoe flows. At Rock Creek (Fig. 5) the oldest exposed Roza lavas pass upwards into clastogenic lava and densely welded spatter. We infer that these fountain-fed clastogenic lavas came from the Rock Creek vent during early phases of the eruptions.

Explosive pyroclastic eruptions seemed to have occurred early on at each vent. This vigorous activity shed clasts from tall fountains and from the lower parts of convective columns and built-up broad cones composed of moderately to densely agglutinated scoria and spatter and lava-like densely welded spatter that extended > 750 m away from the vent (Fig. 10). Buoyant plumes above vigorous fountains dispersed scoria and ash away from the vents. Numerous closely-spaced vents for explosive activity along the fissure led to the convergence and overlap of pyroclastic deposits, building up complex proximal agglutinate cone morphologies and stratigraphies (cf. Thordarson and Self, 1998). Rootless lavas flowing away from the bases of the fountains periodically breached the growing cones and rafted sectors of them away. Based solely on probable minimum accumulation rates, each of these periods of high intensity activity lasted for > 5 to 13 hours at each vent. However, the pyroclastic material preserved in the edifices constitutes only a very small fraction (< 1 %) of the erupted mass: a much greater mass may have been emplaced as clastogenic lavas during these high intensity phases because much material falling at high accumulation rates rapidly coalesces and flows away from the vent, as seen at Laki (Thordarson and Self, 1993). Thus, these phases may have been longer-lived and we cannot constrain how many of these phases there were during the Roza eruption. Through a lack of evidence to the contrary we presently favor a scenario where the bulk of the mass of the Roza Member was effused by long-lived, low intensity fountains. The whole Roza eruption lasted for years to perhaps several decades (Thordarson and Self, 1998) and during this time inflating sheet lobes partially to totally buried the pyroclastic edifices.

Conclusions

The 15 Ma Roza Member has the best exposed vent system and associated pyroclastic deposits of any flood basalt flow field. Investigations of its proximal pyroclastic deposits reveal that the eruptions constructed unusual, broad edifices, here termed agglutinate cones, composed mostly of moderately to densely agglutinated spatter and scoria. Temporal and spatial changes in fountain structure, clast temperature and clast accumulation rate are recorded by complex and rapid facies changes in the deposits that constitute the cones. These edifices have minimum radii of 200–500 m and minimum reconstructed heights of 15–160 m, and may represent a new type of basaltic pyroclastic edifice not previously documented in the literature. The recorded volcanic activity does not fit with presently known eruption styles of basaltic magmas and we infer that the cones were constructed during unusually vigorous explosive phases. Clasts fell out of tall (>> 1 km-high) fountains as well as from the margins of the lower portions of strongly convective columns. Well sorted, highly vesicular scoria lapilli and ash fell out from umbrella regions of these columns. These explosive phases are interpreted to have been relatively short-lived phenomenon that may have emplaced only a fraction (>10 km^3 DRE) of the total erupted mass of the Roza Member. As well as providing the first detailed descriptions of flood-basalt proximal vent edifices and deposits, the outlined geological evidence suggests that the Roza eruption was periodically and repeatedly capable of injecting climate-altering gases high into the atmosphere.

Acknowledgements

This research was funded by NERC standard grant NE/E019021/1 awarded to SS at The Open University. RJB thanks Linda, Henry, Harry and Herman Harder for help, lodgings, beer and access to their land. Marvin Lamb, Ed Knott, Mike Holliday, Charmaine Despain, and Dave and John Schlomer are thanked for generous and unrestricted access to private land. Reviews by X and X. Jw/dg/Sr/Ph.

References

Aramaki, S., Hayakawa, Y., Fujii, T., Nakamura, K., Fukuoka, T., 1986. The October 1983 eruption of Miyakejima volcano. J. Volcanol. Geotherm. Res. 29, 203-229.

Bretz, J.H., Smith, H.T.U., Neff, G.U., 1956. Channelled scabland of Washington—new data and interpretations. Geol. Soc. Am. Bull., 67, 957-1049.

Camp, V.E., Ross, M.E., 2004. Mantle dynamics and genesis of mafic magmatism in the intermontane Pacific Northwest. J. Geophys. Res., 109, B08204. doi:10-1029/2003JB002838.

Camp, V.E., Ross, M.E., Hanson, W.E., 2003. Genesis of flood basalts and Basin and Range volcanic rocks from the Steens Mountain to the Malheur River Gorge, Oregon. Geol. Soc. Am. Bull. 115, 105–128.

Costantini, L., Bonadonna, C., Houghton, B.F., Wehrmann, H., 2009. New physical characterisation of the Fontana Lapilli basaltic Plinian eruption, Nicaragua. Bull. Volcanol. 71, 337-355.

Costantini, L., Pioli, L., Bonadonna, C., Clavero, J., Longchamp, C., 2011. A Late Holocene explosive mafic eruption of Villarica volcano, Southern Andes: the Chamilla deposit. J. Volcanol. Geotherm. Res. 200, 143-158.

Courtillot, V. Renne, P., 2003. On the ages of flood basalt events, Comptus Rendus Geosci. 335, 113-140.

Head, J.W., Wilson, L., 1989. Basaltic pyroclastic eruptions: influence of gas release patterns and volume fluxes on fountain structure, and the formation of cinder cones, spatter cones, rootless flows, lava ponds and lava flows. J. Volcanol. Geotherm. Res., 37, 261-271.

Heliker, C., Kauahikaua J., Sherrod, D.R., Lisowski, M., Cervelli, P., 2003. The rise and fall of Puʻu ʻŌʻō Cone, 1983-2002. In: Heliker, C., Swanson, D.A., Takahashi, T.J., (Eds). The Puʻu ʻŌʻō - Kūpainaha eruption Kīlaeua volcano, Hawaiʻi: the first 20 years. USGS Prof. Paper 1676, 29-52,

Hon, K., Kauahikaua, J., Denlinger R., Mackay, K., 1994. Emplacement and inflation of pāhoehoe sheet flows: observations and measurements of active lava flows on Kilauea Volcano, Hawaii. Geol. Soc. Am. Bull., 106, 351-370.

Hooper, P.R., and Conrey, R.M., 1989. A model for the tectonic setting of the Columbia River basalt eruptions. In: Reidel, S.P., and Hooper, P.R., eds., Volcanism and tectonism in the Columbia River flood basalt province: Geol. Soc. Am. Spec. Paper, 239, 293-306.

Houghton, B. F., Wilson, C.J.N., 1989. A vesicularity index for pyroclastic deposits. Bull. Volcanol., 51, 451-462

Houghton, B.F., Wilson, C.J.N., Fierstein, J., Hildreth, W., 2004. Complex proximal deposition during the Plinian eruptions of 1912 at Novarupta, Alaska. Bull. Volcanol. 66, 95-133.

Houghton, B.F., Gonnermann, H.M., 2008. Basaltic explosive volcanism: constraints from deposits and models. Chemie der Erde, 68, 117-140.

Lund, K., and Snee, L.W., 1988. Structural development and age of the continent-island arc juncture in west-central Idaho: in Ernst, W.G., (Ed) Metamorphism and crustal evolution of the western United States, Prentice-Hall, Englewood Cliffs, 296-331.

Mannen K., Ito, T., 2007. Formation of scoria cone during explosive eruption at Izu-Oshima volcano, Japan. Geophys. Res. Lett., 34, L18302, ODI:10.1029/2007GL030874.

Martin, B.S., 1989. The Roza Member, Columbia River Basalt Group: Chemical stratigraphy and flow distribution. In: Reidel, S.P., and Hooper, P.R., eds., Volcanism and tectonism in the Columbia River flood basalt province: Geol. Soc. Am. Spec. Paper, 239, 85–104.

Olsen, P.E., 1999. Giant lava flows, mass extinctions, and mantle plumes, Science, 293, 604-605.

Parcheta, C.E., Houghton, B.F., Swanson, D.A., 2012. Hawaiian fissure fountains 1: decoding deposits—episode 1 of the 1969-1974 Mauna Ulu eruption. Bull. Volcanol. DOI: 10.1007/s00445-012-0621-1.

Porter, S.C., 1972. Distribution, Morphology, and size frequency of cinder cones on Mauna Kea volcano, Hawai'i. Geol. Soc. Am. Bull., 83, 3607-3612.

Pyle, D.M., 1989. The thickness, volume and grainsize of tephra fall deposits. Bull Volcanol. 51, 1-15.

Rampino M.R., Stothers R.B., 1988. Flood basalt volcanism during the past 250 million years. Science, 241, 663-668.

Reidel, S.P., 1984. The Saddle Mountains—the evolution of an anticline in the Yakima fold belt. American Journal of Science, 284, 942-978.

Reidel, S.P., & Tolan, T.L. 1992. Eruption and emplacement of flood basalt: An example from the large- volume Teepee Butte Member, Columbia River Basalt Group. Geol. Soc. Am. Bull., 104, 1650-1671.

Ross, P.-S. Ukstins Peate T, I., McClintock M.K., Xu, Y.G. Skilling, I.P. White, J.D.L. Houghton B.F., 2005. Mafic volcaniclastic deposits in flood basalt provinces: A review. J. Volcanol. Geotherm. Res., 145, 281– 314

Sable, J.E., Houghton, B.F., Wilson, C.J.N., Carey, R.J., 2006. Complex proximal sedimentation from Plinian plumes: the example of Tarawera 1886. Bull. Volcanol. 69, 89-103

Saunders, A., Reichow, M. 2009. The Siberian Traps and the end-Permian extinction: a critical review. Chin. Sci. Bull. 54, 20-37.

Sparks, R.S.J., Wright, J.V., 1979. Welded air fall tuff. In: Chapin CE, Elston WE (Eds), Ash flow tuffs. Spec. Paper Geol. Soc. Am., 180, 155-166.

Sparks R.S.J. Bursik M.I., Carey. S.N., Gilbert, J.S., Glaze, L.S., Sigurdsson, H., Woods, A.W., 1997. Volcanic plumes. Wiley, pp. 590.

Stothers, R.B., Wolff, J.A., Self, S., Rampino, M.R., 1986. Basaltic fissure eruptions, plume heights, and atmospheric aerosols. Geophys. Res. Lett. 13, 725-728.

Sumner, J.M., 1998. Formation of clastogenic lava flows during fissure eruption and scoria cone collapse: the 1986 eruption of Izu-Oshima volcano, eastern Japan. Bull. Volcanol. 60, 195-212.

Sumner, J.M. Blake S., Matela R.J., Wolff J.A., 2005. Spatter. J. Volcanol. Geotherm. Res. 142, 49-65.

Swanson, D.A., Wright, T.L., and Helz, R.T., 1975. Linear vent systems and estimated rates of magma production and eruption for the Yakima basalt of the Columbia plateau. American Journal of Science, 275, 877-905.

Thomas, R.M.E., Sparks, R.S.J., 1992. Cooling of tephra during fallout from eruption columns. Bull. Volcanol. 54, 542-553.

Thordarson, T., 1991. The 1783–84 Laki eruption: Tephra production and course of events. University of Iceland Special Publication, F90018. University of Iceland Press, Reykjavik, 187p.

Thordarson, T., Self, S., 1993. The Laki (Skaftár Fires) and Grímsvötn eruptions in 1783–1785. Bull. Volcanol. 55, 233–263.

Thordarson, T., Self, S., 1996. Sulfur, chlorine and fluorine degassing and atmospheric loading by the Roza eruption, Columbia River Basalt Group, Washington, USA. J. Volcanol. Geotherm. Res., 74, 49-73.

Thordarson, T., and Self, S., 1998. The Roza Member, Columbia River Basalt Group: a gigantic pahoehoe lava flow field formed by endogenous processes. Journal of Geophysical Research, 103, 27,411-27,445.

Thordarson, T., Miller, D.J., Larsen, G., Self, S., Sigurdsson, H., 2001. New estimates of sulfur degassing and atmospheric mass-loading by the 934 Eldgjá eruption, Iceland. J. Volcanol. Geotherm. Res., 108, 33-54.

Thordarson, T., Rampino, M., Keszthelyi, L.P., Self, S., 2009. Effects of megascale eruptions on Earth and Mars. In: Chapman, M.G., Keszthelyi, L.P., eds, Preservation of random megascale events on Earth and Mars: influence on geologic history. Geol. Soc. Am. Spec. Paper, 453, 37-53.

Tolan, T.L., Beeson, M.H., Anderson, J.L., Fecht, K.R., and Swanson, D.A., 1989. Revisions to the estimates of the areal extent and volume of the Columbia River Basalt Group. Geol. Soc. Am. Spec. Paper, 239, 1-20.

Tolan, T.L., Martin, B.S., Reidel, S.P., Kauffman, J.D., Garwood, D.L., and Anderson, J.L., 2009. An introduction to the stratigraphy, structural geology and hydrogeology of the Columbia River Flood-basalt Province: a primer for the GSA Columbia River Basalt Group field trips. In: O'Conner, J., (Ed) Volcanoes to vineyards: geologic field trips through the dynamic landscape of the Pacific Northwest, GSA Field Guides, 15, 599-643.

Vergniolle, S., Caplan-Auerbach, J., 2006. Basaltic thermals and Subplinian plumes: constraints from acoustic measurements at Shishaldin volcano, Alaska. Bull. Volcanol. 68, 611-630.

Walker, G.P.L., Self, S., Wilson, L., 1984. Tarawera 1886, New Zealand—a basaltic Plinian fissure eruption. J. Vo. 60, 432-440.

Wolfe, E.W., Neal, C.A., Banks, N.G., Duggan, T.J., 1988. The Puu Oo eruption of Kilauea volcano, Hawai´i: episodes 1 through 20, January 3, 1983, through June 8, 1984. US Geol. Surv. Prof. Paper 1463.

Wolff, J.A., Ramos, F.C., Hart, G.L., Patterson, J.D., and Brandon, A.D., 2008. Columbia River flood basalts from a centralized crustal magmatic system. Nature Geosci. 1, 177-180.

Wolff, J.A., Sumner, J.M., 2000. Lava fountains and their products. In: Sigurdsson, H., Houghton B.F., McNutt, S.R., Rymer, H., Stix, J., Encyclopedia of Volcanoes, Academic Press, San Diego, 321-330.

Wood, C.A., 1980. Morphometric evolution of cinder cones. J. Volcanol. Geotherm. Res. 7, 387–413.

Woods, A.W., 1993. A model of the plumes above basaltic fissure eruptions. Geophys. Res. Lett. 20, 1115-1118.

Figure Captions

Figure 1. A. Sketch map of the Columbia River Basalt Province (grey shaded), showing the extent of the Roza Member (solid white line) and the Roza vent system (black solid line). WISZ – Western Idaho Shear Zone marks the location of the continental suture. Large grey oval is the inferred position of the CRBP basaltic magma storage zones/source region according to Wolff et al. (2008). Dotted ovals are dikes swarms: M – monument dike swarm; CJ Chief Joseph dike swarm. B. Map of the northern end of the Roza vent system (area enclosed in rectangle on A) showing outcrops of pyroclastic rocks and names of recognized vent accumulations.

Figure 2. Pyroclastic lithofacies of the Roza Member (see also Table 1 and Fig. 1 for locations). A) Non-welded scoria fall deposit (ScL, Winona). B) Weakly agglutinated scoria lapilli (waScL, Rock Creek Center). C) Moderately agglutinated scoria lapilli (maScL) and spatter bombs (Sp; Buffalo Spring South). Scale in centimeters. D) Densely agglutinated scoria (dwScL) with pronounced columnar joints (Texas Draw). Base of unit is marked by arrows. E) Densely agglutinated spatter (dwSpB; Texas Draw). F) Lava-like densely welded spatter with wispy streaky fiamme (llwSp, Texas Draw). G) Clastogenic lava with heterogeneous patchy vesiculation (clLava, Texas Draw). H)

Pyroclastic lithic breccia composed of Roza lava overlain by non-welded scoria fall deposit (Rock Creek Center, see Fig. 1 and 6). Rule with 10 cm divisions.

Figure 3. Microtextural features of the Roza pyroclastic rocks seen in thin section. Site locations mentioned are shown on Fig. 1. A) Pristine scoria fall deposit from Winona (see also Fig 2A). Clast has a density of 720 kg/m^3 corresponding to a vesicularity of ~75 vol. %. B) Achneliths (Pele's tears) in moderately agglutinated fall deposit at Rock Creek East (Fig 1). Note the moderate amount of welding compaction of clasts. C) Densely agglutinated spatter deposit (Texas Draw, see also Fig 2E). Note moderate, welding-induced, bedding-parallel alignment of plagioclase phenocrysts sitting in a microcrystalline groundmass.

Figure 4. Pyroclastic deposits of the Buffalo Spring North (BSN) and Buffalo Spring South (BSS) vent accumulations: A) Panorama looking east of Buffalo Spring south vent constructs, showing dipping beds and onlapping Roza sheet lobes. Cattle and telegraph pole for scale. B) Geological map of BSN vent deposits that form part of edifice with flanks dipping to NW, W and SW. C) Geological map of BSS vent deposits which form SW end of edifice with flanks dipping to SE, E and S. See key for details. Steep inward dipping beds are inferred to mark the position of the crater. D) Measured section through BSN showing lithological, density and clast flattening ratios with height (abbreviations are explained in Table 1).

Figure 5. Pyroclastic deposits of the Rock Creek vent accumulations. A) Panorama looking east of the Rock Creek Center (RCC) deposits, showing pyroclastic beds thinning southwards over early Roza lavas. B) Cross-section through the RCE edifice with interpretation for how it may have originally looked. C) Dipping beds of predominantly weakly and moderately agglutinated scoria (RCC). E) Geological map of Rock Creek showing the west, center and east vents.

Figure 6. Measured sections through the Rock Creek Center cone deposits (see also Fig. 5), showing variation with height in lithology, grainsize (solid black line), density (average and range of 10 measurements) and clast aspect ratio (average of 10 measurements). Abbreviations for lithofacies are given in Table 1.

Figure 7. Pyroclastic deposits of the Texas Draw (TD) vent accumulations (see Fig. 1 for location of site). A) Photo-interpretation of the pyroclastic edifice at TD, looking west. B) Geological map of Texas Draw (see Fig. 4 for key). Note rapidly changing dips and strikes in the southern half of map. C) Composite section through the southern half of the pyroclastic edifice (see A) showing vertical changes in lithology, density, clast aspect ratio and grainsize. D) Bedded sequence of weakly to densely agglutinated scoria on west side of TD. Ruler for scale, divisions = 10 cm. E) dipping strata at northern end of TD edifice. Horizontal sheet lobes in the distance onlap against the edifice. For key see Fig. 4.

Figure 8. Pyroclastic deposits at the Winona vent (see Fig. 1 for location of site). A) Geological map of the pyroclastic deposits immediately south and east of Winona (see Fig. 4 for key) X-Y-Z is line of section in B; X also marks location of Winona village. B) Scaled cross-section (4 × vertical exaggeration) through the Winona vent accumulations. Note the opposing flanks of densely agglutinated spatter terminating abruptly at the inferred vent. C) Eastern spatter mound with fiamme (arrows) dipping gently to the east. For key see Fig. 4.

Figure 9. A) Histogram of dip magnitudes of bedding planes and welding fabrics in pyroclastic deposits around Roza vents. B) Plot of flattening ratio against mean density (average of 10 measurements) for pyroclastic deposits of the Roza Member. C) Histogram of the densities of 16–32

mm scoria lapilli from a scoria fall deposit 1.7 km from vent at Winona (n=100). D) Grainsize distribution of the Roza fall deposit in C compared to similar deposits from historical eruptions. The Laki and Eldgja samples were collected from sites <1.5 km from the vents and are representative for the fall deposit in the proximal/near vent region (Thordarson, 1991).

Figure 10. Cartoon illustrating a sustained convective column developed above a vent in the Roza eruption. Fallout from tall fountains supplemented by fallout from the margins of the lower parts of convective columns result in high aggradation rates (>> 20 cm/min) and the construction of broad wide agglutinate cones dominated by welded and agglutinated deposits.

lithofacies	ρ (kg m^{-3})	clast aspect ratio	description	interpretation
scoria lapilli (ScL)	300–1100	N/A	**Composition:** well-sorted, clast-supported, black, angular moderately to highly vesicular scoria lapilli, bombs and coarse ash; variably altered; clasts exhibit fractured surfaces, fluidal exteriors; achneliths common; **Structure:** massive; rare thin beds defined by slight grainsize variation; occurs in units up to 3 m thick. **Occurrence:** medial fall deposit > 300 m from inferred vents; interbedded with other pyroclastic lithofacies in proximal regions and in between pahoehoe lobes at distances > 500 m from source; coarsens towards source.	Fall deposit from sustained eruption plume above Hawai‘ian fire fountain.
weakly agglutinated scoria lapilli (waScL)	1200–1400	1:1–1:3	**Composition:** As ScL; clasts stuck together at point contacts; **Structure:** massive; small amounts of clast deformation; minor reduction in deposit pore space; occurs in units up to 1 m thick. **Occurrence:** as ScL; proximal and medial deposit.	As above; higher accumulation rates promoted agglutination at point contacts
moderately agglutinated scoria lapilli (maScL)	1200–1800	1:1.3–1:6	**Composition:** moderately well sorted clast-supported scoria lapilli and bombs up to 15 cm in diameter; black to orange (oxidised in color); commonly glass of clasts has been altered to clay. Achneliths common. **Structure:** individual clast outlines visible; moderate deformation of clasts; massive to crudely bedded; bedding defined by grainsize; occurs in units from 0.5–14 m thick **Occurrence:** proximal cone-building deposits and sheet-forming deposits; interbedded with other proximal lithofacies.	Fallout from lava fountain; elevated accumulation rates promoted agglutination.
densely welded scoria lapilli (dwScL)	1500–2200	1:2–1:15	**Composition:** as wScL; clasts up to up to 15 cm; clast outlines poorly visible; variable vesicularity. **Structure:** massive; in beds up to 3 m thick; strong eutaxitic texture; characterised by poor to well developed columnar joints; complete loss of deposit pore space. **Occurrence:** proximal cone-building deposits and sheet-forming deposits.	Fallout from inner parts of lava fountain; rapid accumulation rates promoted dense agglutination and allow cooling joints to form.
densely welded spatter (dwSp)	1700–2800	1:3–1:20	**Composition:** densely welded spatter bombs up to 90 cm. **Structure:** massive; sharp contacts; intense clast deformation with high aspect ratio fiamme; complete loss of pore space; occurs in units from 0.5–10 m thick; **Occurrence:** proximal cone-building deposits.	Fallout of large spatter clasts under inner parts of lava fountain.
lava-like densely welded spatter (llwSp)	2200–2700	N/A	**Composition:** vitrophyric non-vesicular glass; clast outlines not visible; rare wispy vesicular fiamme present in some outcrops; **Structure:** massive; cm-spaced platy joints or poorly developed columnar joints; hackly fracture; occurs in units 2.5–>5 m thick; absence of chilled margins. **Occurrence:** proximal cone-building deposits.	Fallout of fluidal spatter clasts from inner fountain; rapid accumulation rates; clasts coalesce on deposition
clastogenic lava (clLava)	1600–2000	N/A	**Composition:** crystalline lava with irregular distribution of vesicles; outlines of clasts defined by vesicle patches. **Structure:** massive; forms units up to 0.3–2 m thick. **Occurrence:** cone-building deposits and sheet-forming deposits: interbedded with proximal pyroclastic lithofacies.	Coalescence of pyroclasts at base of fountain; flows away as lava.
Breccia (Br)	>2700	N/A	**Composition:** clast-supported angular blocks of lava. **Structure:** massive; poorly exposed **Occurrence:** proximal edifice at Rock Creek Centre vent.	Formed by explosive eruptions; ballistically-emplaced clasts

Table 1. Summary description and interpretation for pyroclastic lithofacies of the Roza Member.

pyroclastic vent	**Location (Deg. Min. Sec)**	**description**
Harder Ranch	47° 4'47.44"N 118° 0'33.80"W	Dipping beds (0–32°) of densely agglutinated scoria and spatter poorly exposed over 0.27 km^2; bedding defines a partial cone with dips to the N, W and SW, an apparent radius of >350 m and length of >500 m; oldest deposits are lava-like densely welded spatter; spatter bombs > 50 cm in diameter; base of pyroclastic deposits not seen; onlapped by Roza sheet lobes and Rosalia Member.
Rock Creek North	47° 2'39.51"N 117°57'9.64"W	Bedded moderately to densely agglutinated scoria and spatter outcropping over 0.1 km^2; Bedding dips (3–31°) define a half-cone with slopes to the NW, N and NE, a radius of ~250 m and a length of 450 m; ropey-surfaced vesicular spatter bombs reach 45 cm in diameter; onlapped by Roza sheet lobes.
Rock Creek West	47° 1'2.01"N 117°57'2.31"W	4 m of lava-like densely welded spatter passing up into 5 m of bedded weakly and moderately agglutinated scoria; dense spatter bombs up to 6 m in diameter; vesicular spatter bombs up to 80 cm in diameter; Beds dip north and west and may define a partial cone or drape underlying lava topography; overlies Roza sheet lobe (as Rock Creek Center).
Palouse River	46°55'13.10"N 117°50'48.42"W	Flat-lying beds of moderately to densely agglutinated spatter and lava-like spatter exposed in bluffs along Palouse River; rafted spatter ramparts overlie capping Roza sheet lobe.
*Union Flat Creek	46°52'9.84"N 117°45'57.34"W	Small roadcut exposing >2 m of densely agglutinated spatter overlying Roza sheet lobe; thin scoria fall deposit exposed in road cuts to east with welded top.
*Megginson Gulch	46°26'35.71"N 117°24'19.50"W	Discontinuous road cuts through densely welded and agglutinated spatter and spongy pāhoehoe lobes.
*Potter White Hill [15]	46°19'15.00"N 117°21'8.81"W	Road cut and small quarry in moderately to densely welded spatter and chaotic agglutinate meso-breccias; interpreted as crater deposits (Brown et al., in press).
*Little Butte [16]	46° 8'29.92"N 117°16'20.41"W	Poorly exposed densely welded spatter and dense lava interpreted as lava shield volcano (Swanson et al., 1975)
*Big Butte [17]	46° 6'52.25"N 117°15'10.94"W	As Little Butte.
Crow Creek	45°37'28.37"N 117° 8'23.14"W	Road cuts and borrow pit through steeply dipping non-welded fall deposits, moderately to densely agglutinated scoria and spatter, spongy pāhoehoe, clastogenic lava and breccia; deposits occur within conduit cut through Grande Ronde lavas; interpreted as conduit deposits.

Table 2. Summary information for poorly exposed vents and pyroclastic deposits of the Roza Member not described in the text and arranged from north to south. *localities of Swanson et al., (1975); numbers in square brackets are their numbering scheme. For location see Figure 1C.

Vent	**Location**	**[1]masl**	**[2]trend**	**[3]l (km)**	**[4]r (km)**	**[5]area (km^2)**	**$\theta_{min-max}$**	**θx**	**θ σ**	**[6]h_{min} (m)**	**[7]h_{max} (m)**
Harder Ranch	47° 4'50.28"N 118° 0'32.17"W	513	NNE-SSW	0.5	0.35	0.27	2–32°	17°	8°	53	107
Buffalo Spring (N)	47° 4'15.20"N 117°59'46.17"W	495	N-S	0.56	0.33	0.29	6–35°	15°	6°	51	88
Buffalo Spring (S)	47° 3'49.75"N 117°59'7.17"W	485	N-S	0.28	0.2	0.08	6–31°	16°	8°	50	57
Rock Creek (N)	47° 2'35.65"N 117°57'11.64"W	495	NNE-SSW	0.43	0.25	0.17	3–31°	19°	8°	46	86
Rock Creek (C)	47° 1'13.37"N 117°56'41.91"W	460	NNW-SSE	0.5	0.22	0.17	*12–24°	-	-	30	63
Rock Creek (E)	47° 1'26.86"N 117°56'6.48"W	480	NNE-SSW	0.41	0.23	0.15	13–44°	19°	9°	40	79
Texas Draw	46°58'47.63"N 117°52'55.02"W	480	N-S	0.56	0.22	0.19	6–37°	16°	8°	35	63
Mason Draw	46°57'4.11"N 117°51'3.91"W	470	NNE-SSW	0.9	0.5	0.71	9–27°	18°	7°	25	162
Winona	46°56'26.34"N 117°48'47.97"W	450	-	-	0.42	-	5–9°	-	-	15	15

Table 3. Dimensions of pyroclastic cone remnants at vent localities. Orientation of cones estimated from bedding and foliation dips. [1]altitude of lowest exposed pyroclastic bed; [2]parallel to elongation of cone structure; [3]length parallel to cone structure/trend of fissure; [4]radius - orthogonal radius; [5]equivalent ellipse ($a = 0.5 \pi r l$) [6]minimum height of cone using 460 m altitude as datum (base of pyroclastic successions at Winona and Rock Creek); [7]reconstructed by projecting average welding foliation dips (θx). *limited data; dip of 16° used to calculate h_{max}.

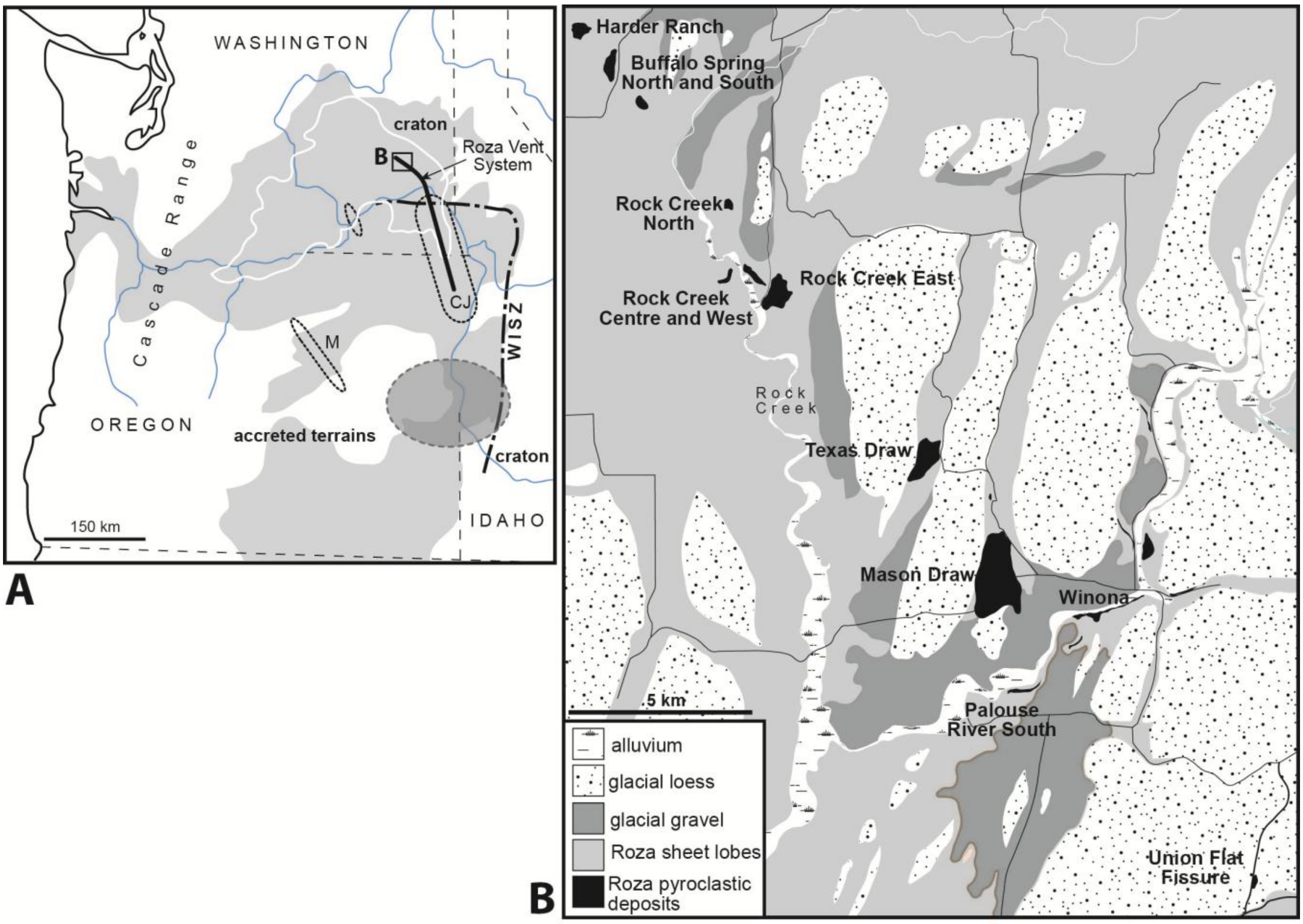
WASHINGTON
craton
B
Roza Vent
System
Cascade Range
CJ
M
WISZ
OREGON
accreted terrains
craton
150 km
IDAHO
A
Harder Ranch
Buffalo Spring
North and South
Rock Creek
North
Rock Creek East
Rock Creek
Centre and West
Rock
Creek
Texas Draw
Mason Draw
Winona
5 km
Palouse
River South
Union Flat
Fissure
alluvium
glacial loess
glacial gravel
Roza sheet lobes
Roza pyroclastic
deposits
B

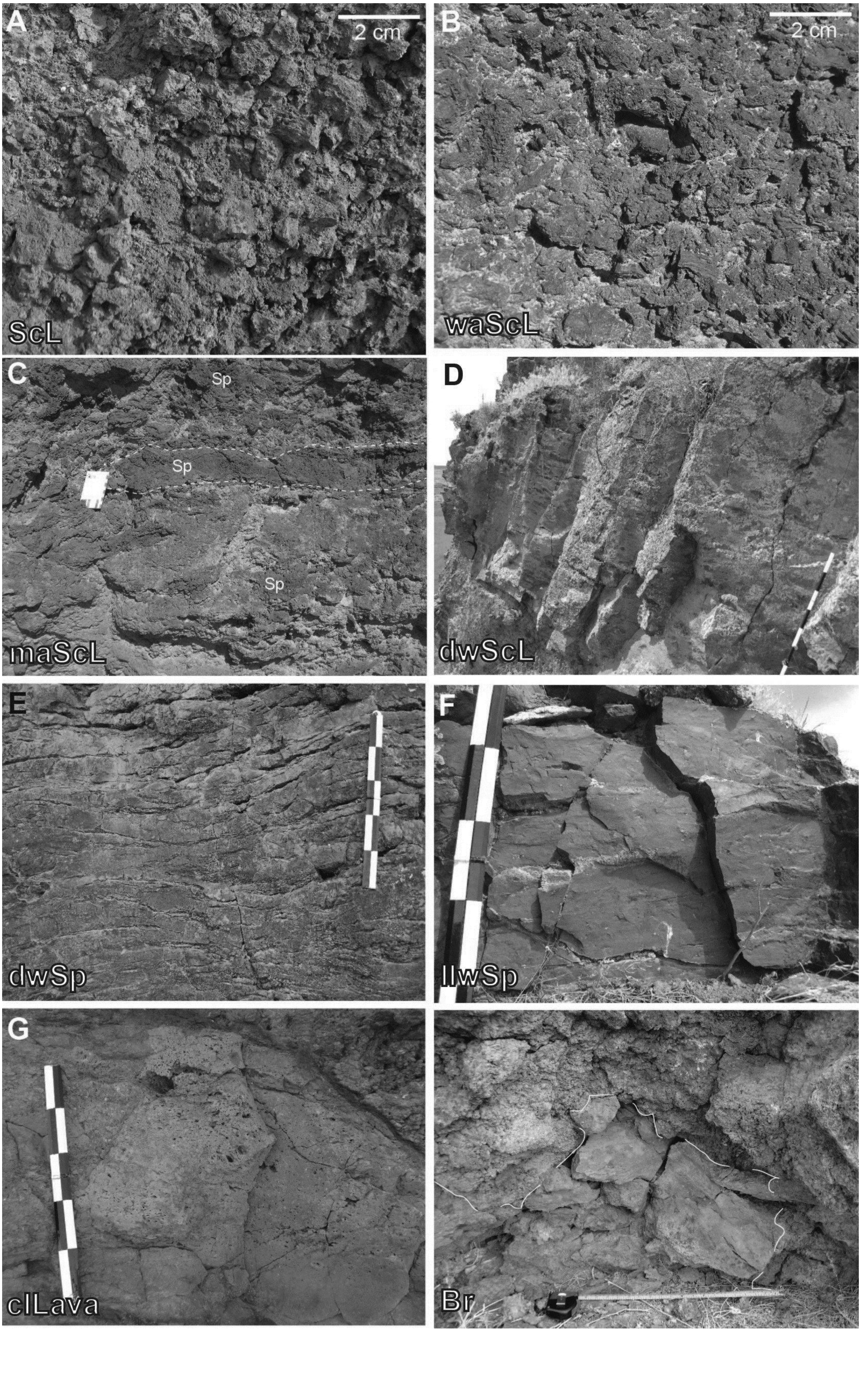
A
2 cm
ScL
B
2 cm
waScL
C
Sp
Sp
Sp
maScL
D
dwScL
E
dwSp
F
llwSp
G
clLava
Br

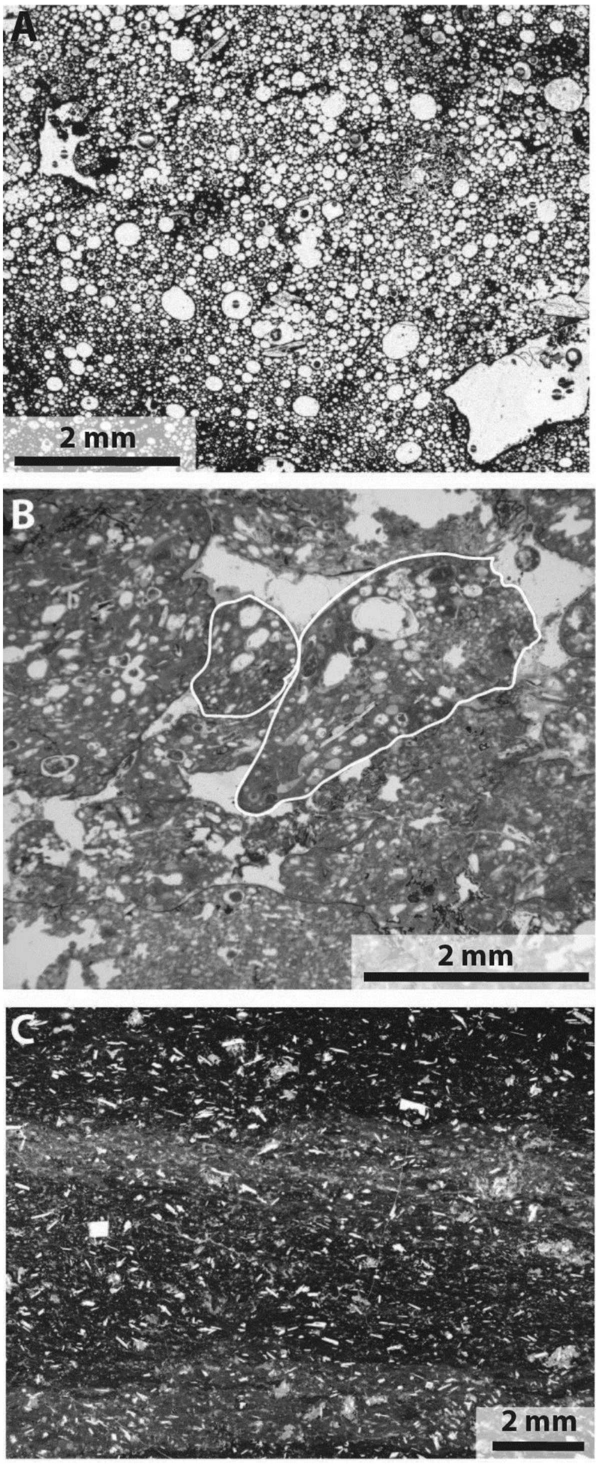
A
2 mm
B
2 mm
C
2 mm

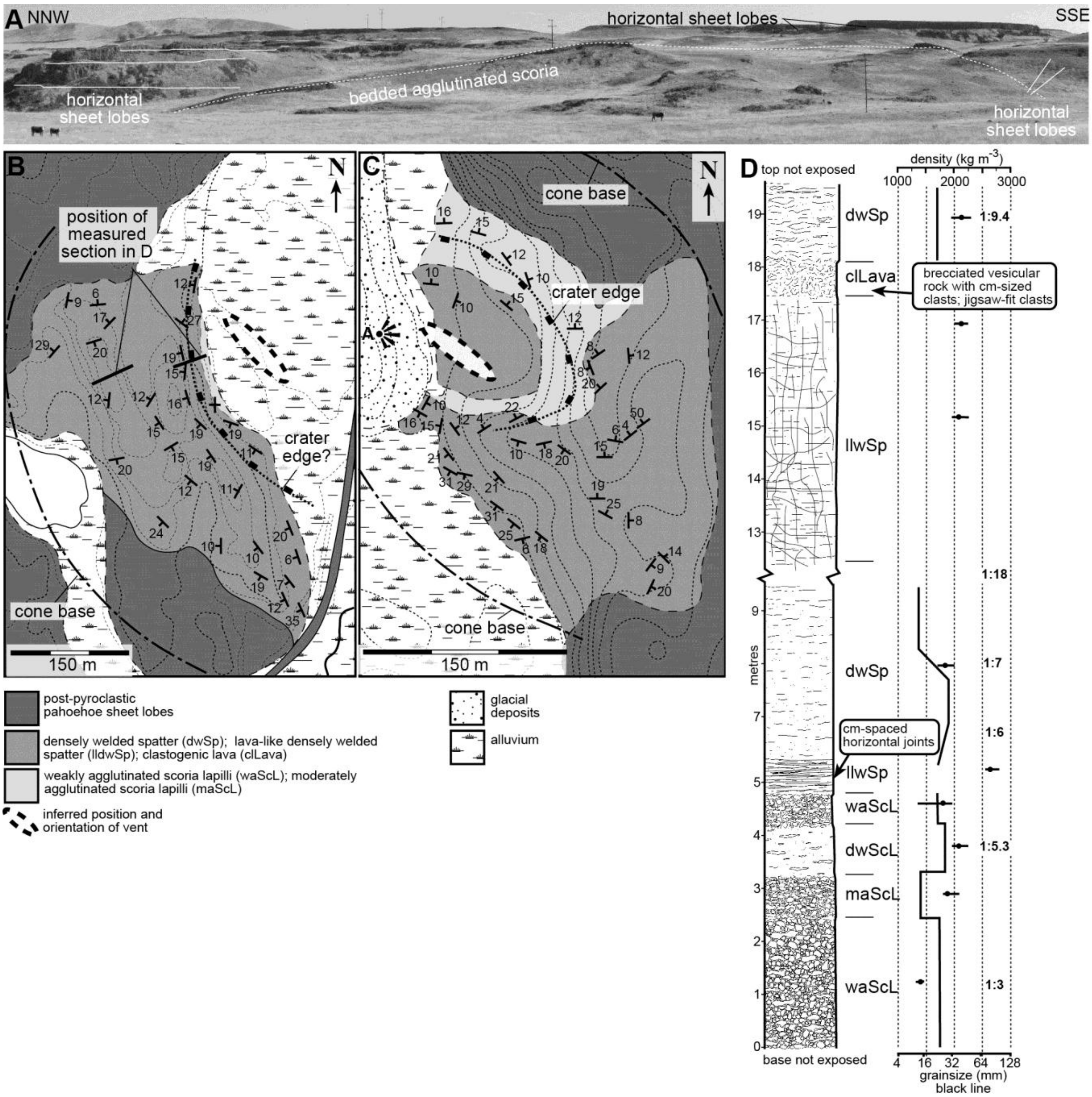
A NNW
SSE
horizontal sheet lobes
bedded agglutinated scoria
horizontal sheet lobes
horizontal sheet lobes
B
position of measured section in D
crater edge?
cone base
150 m
C
cone base
crater edge
cone base
150 m
A
D top not exposed
density (kg m^{-3})
1000 2000 3000
dwSp
1:9.4
clLava
brecciated vesicular rock with cm-sized clasts; jigsaw-fit clasts
llwSp
1:18
dwSp
1:7
1:6
cm-spaced horizontal joints
llwSp
waScL
dwScL
1:5.3
maScL
waScL
1:3
metres
base not exposed
4 16 32 64 128
grainsize (mm)
black line
post-pyroclastic pahoehoe sheet lobes
densely welded spatter (dwSp); lava-like densely welded spatter (lldwSp); clastogenic lava (clLava)
weakly agglutinated scoria lapilli (waScL); moderately agglutinated scoria lapilli (maScL)
inferred position and orientation of vent
glacial deposits
alluvium

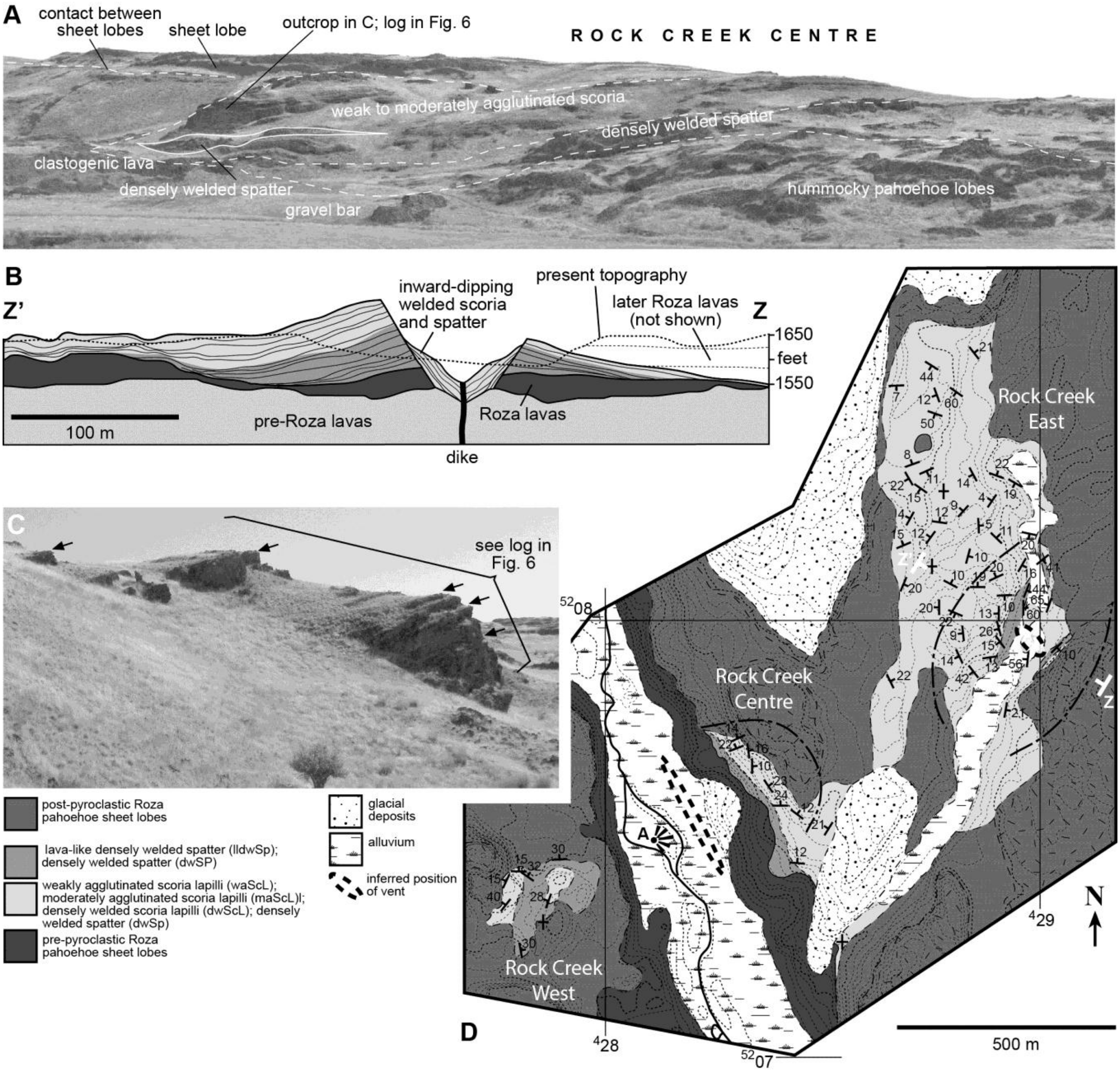

A
contact between sheet lobes
sheet lobe
outcrop in C; log in Fig. 6
ROCK CREEK CENTRE
weak to moderately agglutinated scoria
densely welded spatter
clastogenic lava
densely welded spatter
gravel bar
hummocky pahoehoe lobes
B
Z'
Z
inward-dipping welded scoria and spatter
present topography
later Roza lavas (not shown)
1650
feet
1550
100 m
pre-Roza lavas
Roza lavas
dike
C
see log in Fig. 6
post-pyroclastic Roza pahoehoe sheet lobes
lava-like densely welded spatter (lldwSp); densely welded spatter (dwSP)
weakly agglutinated scoria lapilli (waScL); moderately agglutinated scoria lapilli (maScL)l; densely welded scoria lapilli (dwScL); densely welded spatter (dwSp)
pre-pyroclastic Roza pahoehoe sheet lobes
glacial deposits
alluvium
inferred position of vent
Rock Creek East
Rock Creek Centre
Rock Creek West
A
N
500 m
5208
5207
428
429
D

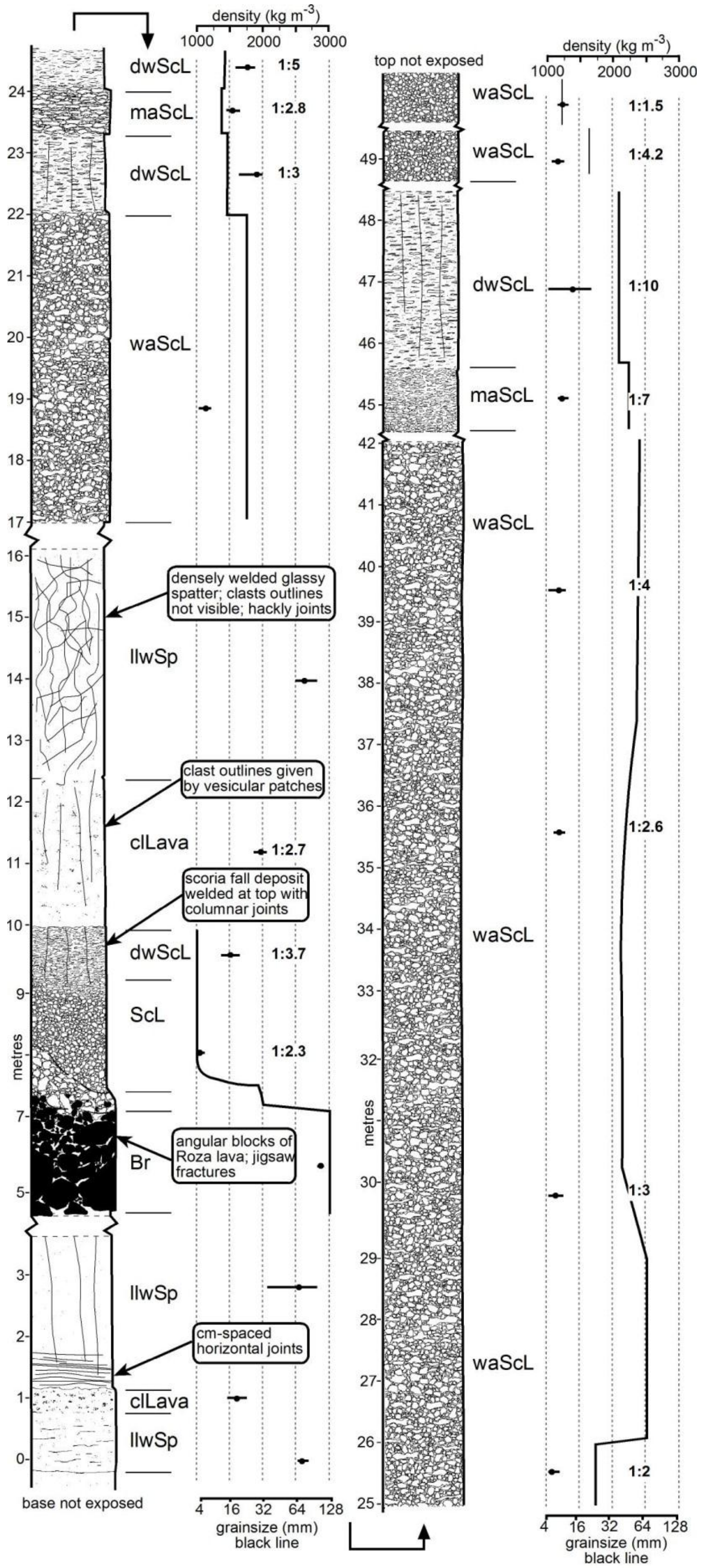

density (kg m^{-3})
1000 2000 3000
dwScL
1:5
maScL
1:2.8
dwScL
1:3
waScL
densely welded glassy spatter; clasts outlines not visible; hackly joints
llwSp
clast outlines given by vesicular patches
clLava
1:2.7
scoria fall deposit welded at top with columnar joints
dwScL
1:3.7
ScL
1:2.3
angular blocks of Roza lava; jigsaw fractures
Br
llwSp
cm-spaced horizontal joints
clLava
llwSp
base not exposed
metres
4 16 32 64 128
grainsize (mm)
black line
top not exposed
waScL
1:1.5
waScL
1:4.2
dwScL
1:10
maScL
1:7
waScL
1:4
1:2.6
waScL
1:3
waScL
1:2

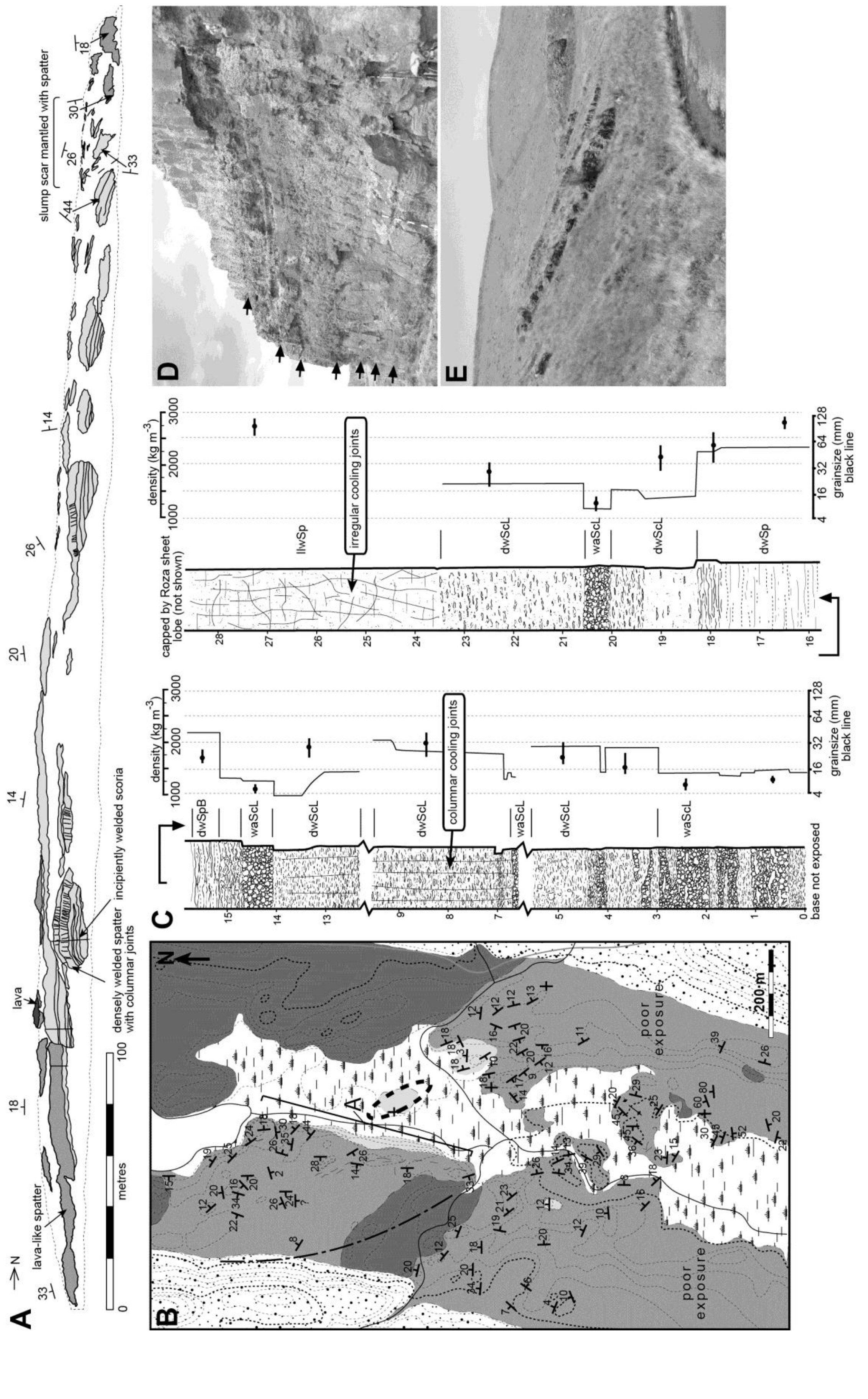
A
lava-like spatter
lava
densely welded spatter with columnar joints
incipiently welded scoria
slump scar mantled with spatter
metres
B
poor exposure
200 m
C
base not exposed
columnar cooling joints
capped by Roza sheet lobe (not shown)
irregular cooling joints
dwSpB
waScL
dwScL
llwSp
dwSp
density (kg m-3)
grainsize (mm) black line
D
E

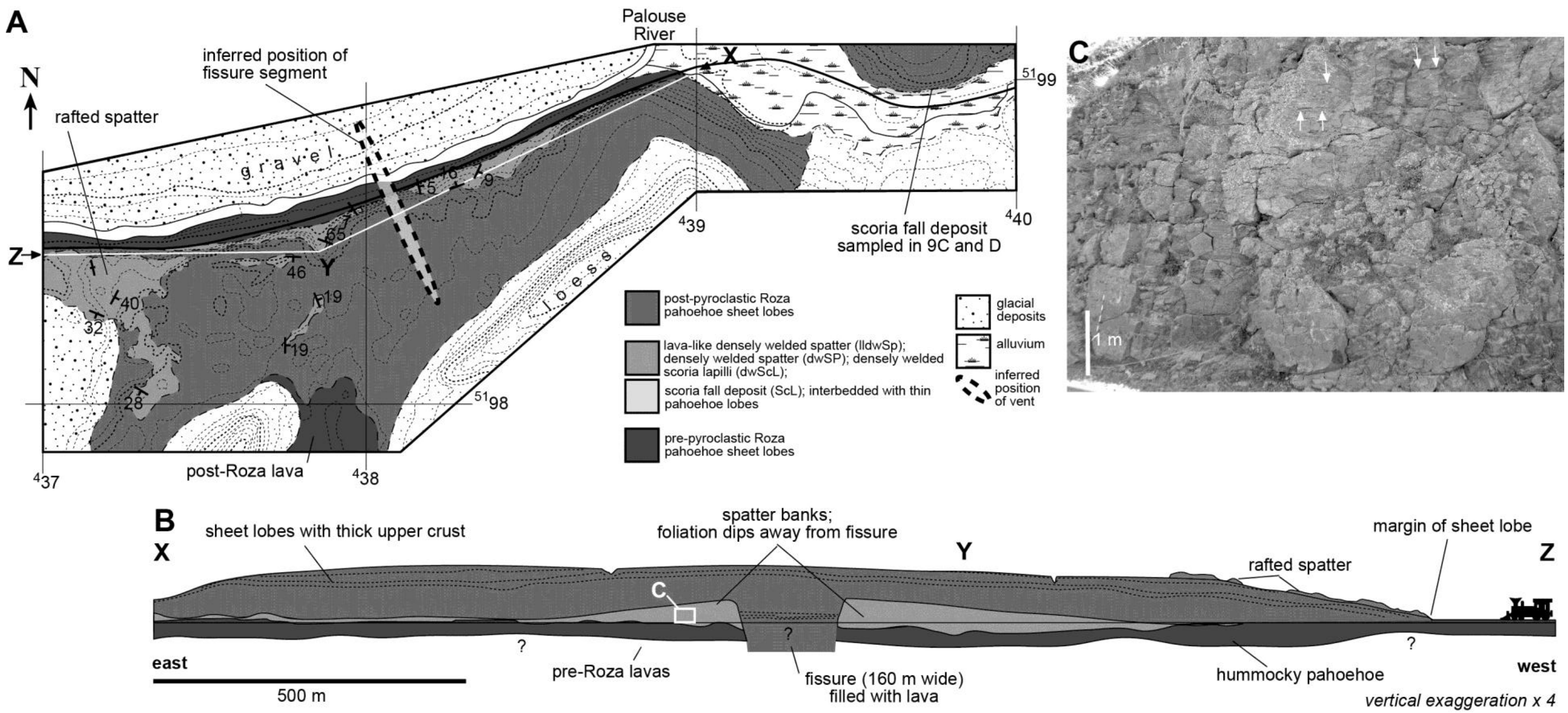
A
N
rafted spatter
inferred position of fissure segment
Palouse River
X
Z
Y
g r a v e l
l o e s s
scoria fall deposit sampled in 9C and D
post-Roza lava
post-pyroclastic Roza pahoehoe sheet lobes
lava-like densely welded spatter (lldwSp); densely welded spatter (dwSP); densely welded scoria lapilli (dwScL);
scoria fall deposit (ScL); interbedded with thin pahoehoe lobes
pre-pyroclastic Roza pahoehoe sheet lobes
glacial deposits
alluvium
inferred position of vent
437
438
439
440
5198
5199
C
1 m
B
sheet lobes with thick upper crust
spatter banks; foliation dips away from fissure
margin of sheet lobe
rafted spatter
east
west
500 m
pre-Roza lavas
fissure (160 m wide) filled with lava
hummocky pahoehoe
vertical exaggeration x 4

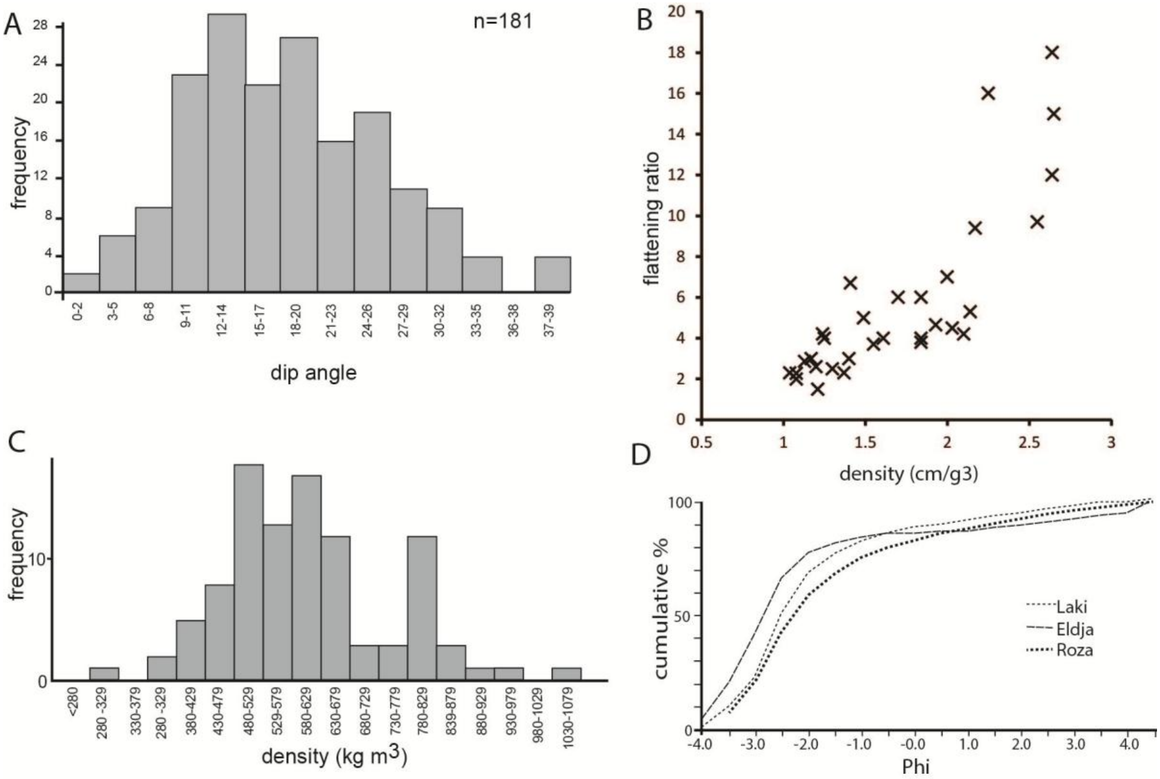
A
n=181
frequency
dip angle
B
flattening ratio
density (cm/g3)
C
frequency
density (kg m3)
D
cumulative %
Laki
Eldja
Roza
Phi

1017

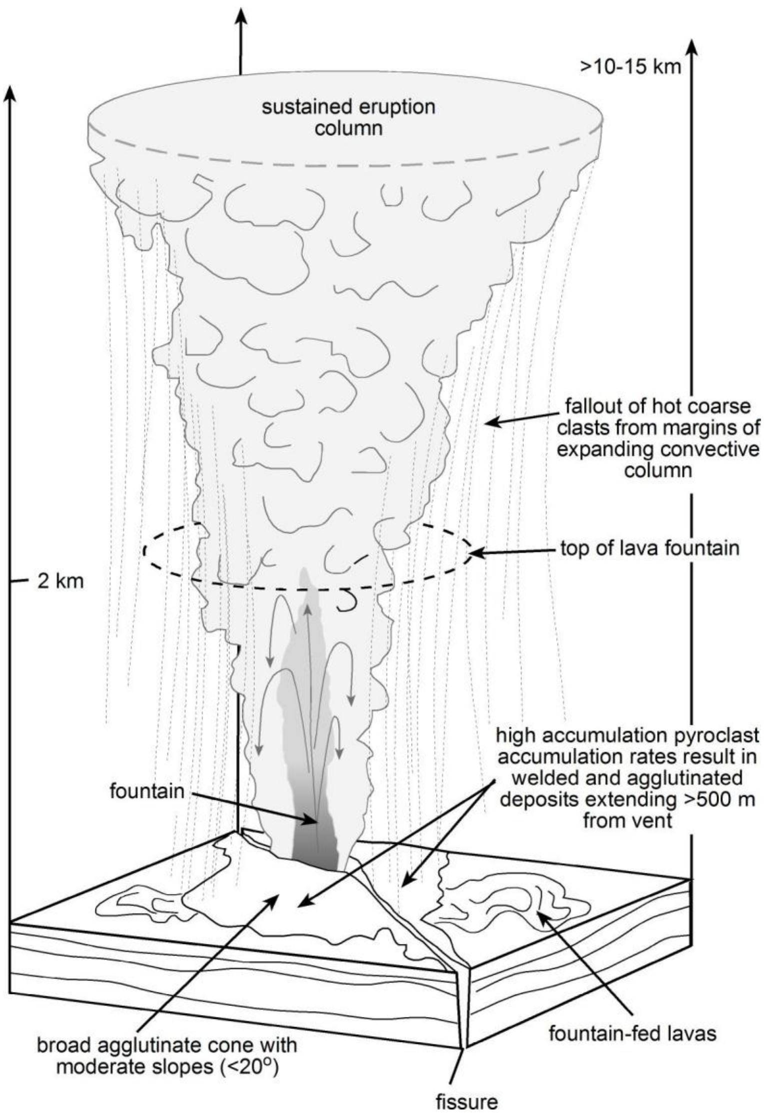

>10-15 km
sustained eruption column
fallout of hot coarse clasts from margins of expanding convective column
top of lava fountain
2 km
high accumulation pyroclast accumulation rates result in welded and agglutinated deposits extending >500 m from vent
fountain
broad agglutinate cone with moderate slopes (<20°)
fountain-fed lavas
fissure